Published in Quarterly Reviews of Biophysics 33, issue 1, 67-108, 2000
which should be used for any reference to this work

How does light regulate chloroplast enzymes? Structure–function studies of the ferredoxin/thioredoxin system

Shaodong Dai[1,3], Cristina Schwendtmayer[2], Kenth Johansson[1], S. Ramaswamy[1,4], Peter Schürmann[2] and Hans Eklund[1]*

[1] Department of Molecular Biology, Swedish University of Agricultural Sciences, Box 590, Biomedical Center, S-751 24 Uppsala, Sweden
[2] Laboratoire de Biochimie Végétale, Université de Neuchâtel, CH-2007 Neuchâtel, Switzerland
[3] Present address: Department of Biological Sciences, 1392 Lilly Hall of Life Sciences, Purdue University, West Lafayette, IN 47907, USA
[4] Present address: Department of Biological Sciences, University of Iowa, Iowa City, IA 52242-1109, USA

* Author to whom correspondence should be addressed.

I. Introduction

A pre-requisite for life on earth is the conversion of solar energy into chemical energy by photosynthetic organisms. Plants and photosynthetic oxygenic microorganisms trap the energy from sunlight with their photosynthetic machinery and use it to produce reducing equivalents, NADPH, and ATP, both necessary for the reduction of carbon dioxide to carbohydrates, which are then further used in the cellular metabolism as building blocks and energy source. Thus, plants can satisfy their energy needs directly via the light reactions of photosynthesis during light periods. The situation is quite different in the dark, when these organisms must use normal catabolic processes like non-photosynthetic organisms to obtain the necessary energy by degrading carbohydrates, like starch, accumulated in the chloroplasts during daylight. The chloroplast stroma contains both assimilatory enzymes of the Calvin cycle and dissimilatory enzymes of the pentose phosphate cycle and glycolysis. This necessitates a strict, light-sensitive control that switches between assimilatory and dissimilatory pathways to avoid futile cycling (Buchanan, 1980, 1991; Buchanan *et al*. 1994; Jacquot *et al*. 1997; Schürmann & Buchanan, 2000).

The activity of ribulose-1,5-bisphosphate carboxylase (Rubisco), fructose-1,6-bisphosphatase (FBPase), sedoheptulose-1,7-bisphosphatase (SBPase) and phosphoribulokinase (PRK), the key enzymes of the Calvin cycle, are controlled by pH, Mg^{2+}, ATP concentration and by the production of Rubisco inhibitor in the dark. In addition, a specific system senses the light-dependent redox potential changes of the stroma and translates them into signals which, in the light, stimulate the Calvin cycle and deactivate catabolic pathways. The light sensitive system exerting such a control function is the ferredoxin/thioredoxin system, composed of ferredoxin, ferredoxin:thioredoxin reductase, thioredoxin and target enzymes (Jacquot *et al*. 1997; Schürmann & Buchanan, 2000) (Fig. 1). Sunlight photons are captured by chlorophyll pigments in the photosystems and used to oxidize water and reduce ferredoxin. The light signal, represented by reduced ferredoxin, is transmitted by ferredoxin:thioredoxin reductase (FTR) to a redox cascade of disulfide–dithiol interchanges, which regulate the activity of target enzymes through the reduction of regulatory disulfides by reduced thioredoxins. The reactions of the reductive pentose phosphate cycle (the Calvin cycle) are usually divided into three phases: carboxylation of ribulose-1,5-bisphosphate, reduction (using ATP and NADPH) and regeneration of ribulose-1,5-bisphosphate. Three of the four light-dependent redox regulation sites are located in the regeneration phase: FBPase, SBPase and PRK. Reactions closely related with carbon assimilation and also activated by light include the synthesis of ATP by the coupling factor ATPase (Mills *et al*. 1980; Schwarz *et al*. 1997), activation of Rubisco activase (Zhang & Portis, 1999), and, in higher plants, starch biosynthesis (Ballicora *et al*. 2000) and the synthesis of malate by NADP–malate dehydrogenase (MDH) (Miginiac-Maslow *et al*. 1997). On the other hand, light inactivates one enzyme of the oxidative pentose phosphate pathway, the glucose-6-phosphate dehydrogenase (G6PDH) (Lendzian & Ziegler, 1970; Wenderoth *et al*. 1997). This regulation prevents simultaneous carbohydrate synthesis in the Calvin cycle and catabolism by the oxidative pentose-phosphate pathway. Thus, in accordance with its

Abbreviations: FTR – ferredoxin:thioredoxin reductase, Rubisco – ribulose-1,5-bisphosphate carboxylase/oxygenase, FBPase – fructose-1,6-bisphosphatase, SBPase – sedoheptulose-1,7-bisphosphatase, PRK – phosphoribulokinase, G6PDH – glucose-6-phosphate dehydrogenase.

Table 1. *Structures of proteins in the ferredoxin:thioredoxin system*

Organism	PDB code	Resolution	Reference
Photosystem I			
Synechococcus Elongatus	2PPS	4·0 Å	Krauss *et al*. 1996 Klukas *et al*. 1999a,b
PsaE			
Synechococcus sp.	1PSE	NMR	Falzone *et al*. 1994
Nostoc sp.	1QP2	NMR	Mayer *et al*. 1999
Ferredoxin			
Parsley	1PFD	NMR	Im *et al*. 1998
Spinach	1A70	1·7 Å	Binda *et al*. 1998
Anabaena sp.	1CZP	1·2 Å	Morales *et al*. 1999
Anabaena sp. 7119	1QT9	1·3 Å	Morales *et al*. 1999
Anabaena sp. 7120	1FXA	2·5 Å	Rypiniewski *et al*. 1991
	1FRD	1·7 Å	Jacobson *et al*. 1993
Aphanothece sacrum	1FXI	2·2 Å	Tsukihara *et al*. 1990
Chlorella fusca	1AWD	1·4 Å	Bes *et al*. 1999
Equisetum arvense	1FRR	1·8 Å	Ikemizu *et al*. 1994
Haloarcula Marismortui	1DOI	1·9 Å	Frolow *et al*. 1996
Spirulina platensis	4FXC	2·5 Å	Fukuyama *et al*. 1980
Synechococcus elongatus	1ROE	NMR	Baumann *et al*. 1996
Synechocystis sp.	1DOX, 1DOY	NMR	Lelong *et al*. 1995
Thioredoxin			
Spinach trx-*f*	1F9M, 1FAA	1·9, 1·8 Å	Capitani *et al*. 1998
Spinach trx-*m*	1FB6, 1FB0	2·1, 2·3 Å	Capitani *et al*. 1998
Anabaena sp. 7120	1TXH	1·7 Å	Saarinen *et al*. 1996
Chlamydomonas reinhardtii	1DBY	NMR	Lancelin *et al*. (unpublished, and 1993)
FTR			
Synechocystis sp.		1·6 Å	Dai *et al*. 2000
FBPase			
Pea	1D9Q	2·4 Å	Chiadmi *et al*. 1999
Spinach		2·8 Å	Villeret *et al*. 1995a
NADP–MDH			
Sorghum vulgare	7MDH	2·4 Å	Johansson *et al*. 1999
Flaveria bidentis	1CIV	2·8 Å	Carr *et al*. 1999

physiological role in chloroplasts, G6PDH is active only at night, when NADPH supply by the photosynthetic electron flow ceases.

Three-dimensional structures of proteins in all steps of the light regulation pathway have now been determined (Table 1), which allows us to outline the process of light regulation at the molecular level. The crystal structure of cyanobacterial PSI (Krauss *et al*. 1996) has recently been improved at 4 Å resolution (Klukas *et al*. 1999a,b) and reveals the overall architecture and the arrangement of most subunits. Several three-dimensional structures of

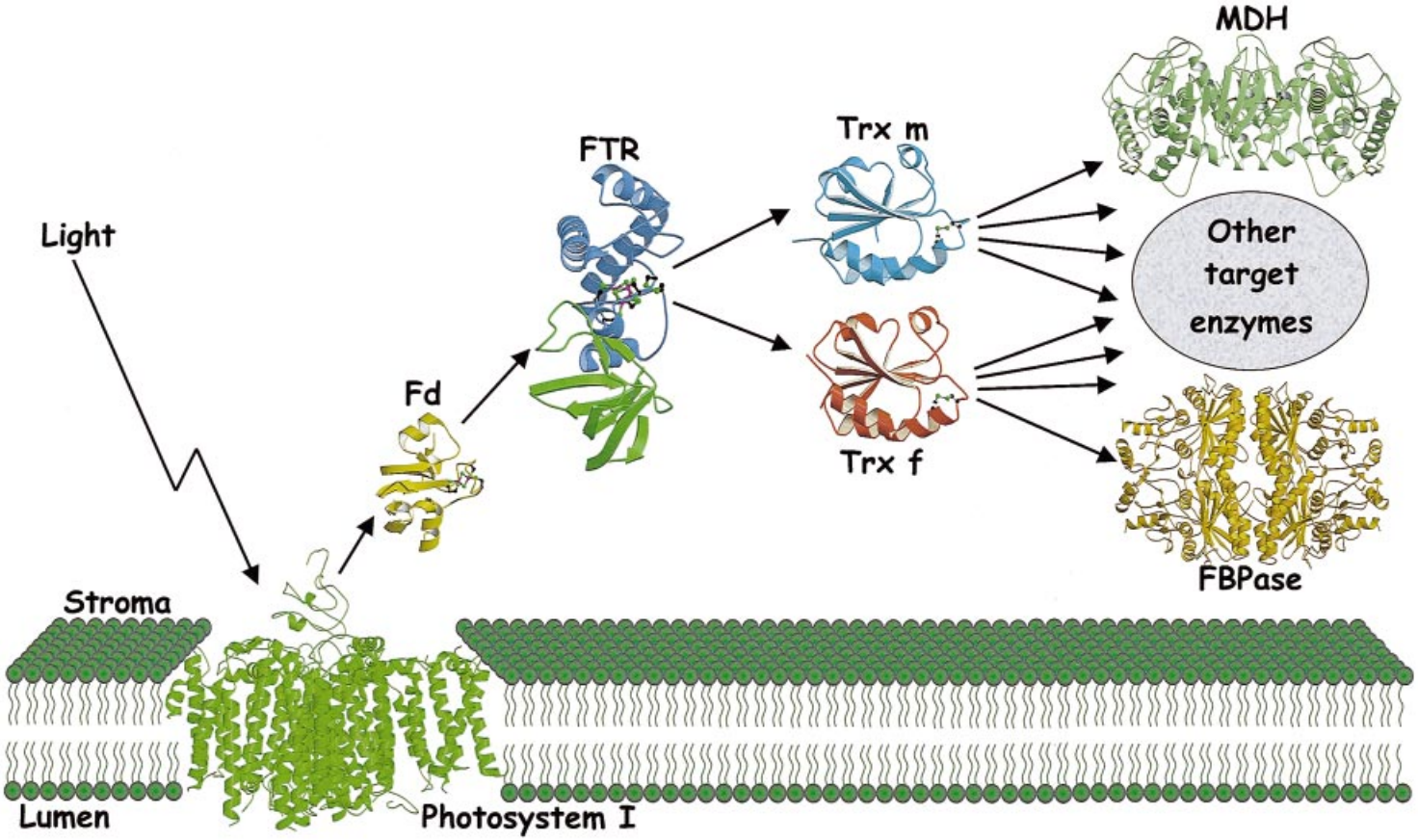

Fig. 1. Light induced enzyme regulation in chloroplasts through the ferredoxin:thioredoxin reductase system. Upon illumination, the photosynthetic electron transfer chain reduces ferredoxin (Fd) by photosystem I. Ferredoxin can then reduce ferredoxin:thioredoxin reductase (FTR) which reduces the chloroplast thioredoxins *m* and *f* (Trx-*m* and Trx-*f*). Finally the thioredoxins activate (in one case deactivate) target enzymes, here exemplified by malate dehydrogenase, (MDH) and fructose-1,6-bisphosphatase (FBPase), thereby changing the metabolism to anabolic pathways.

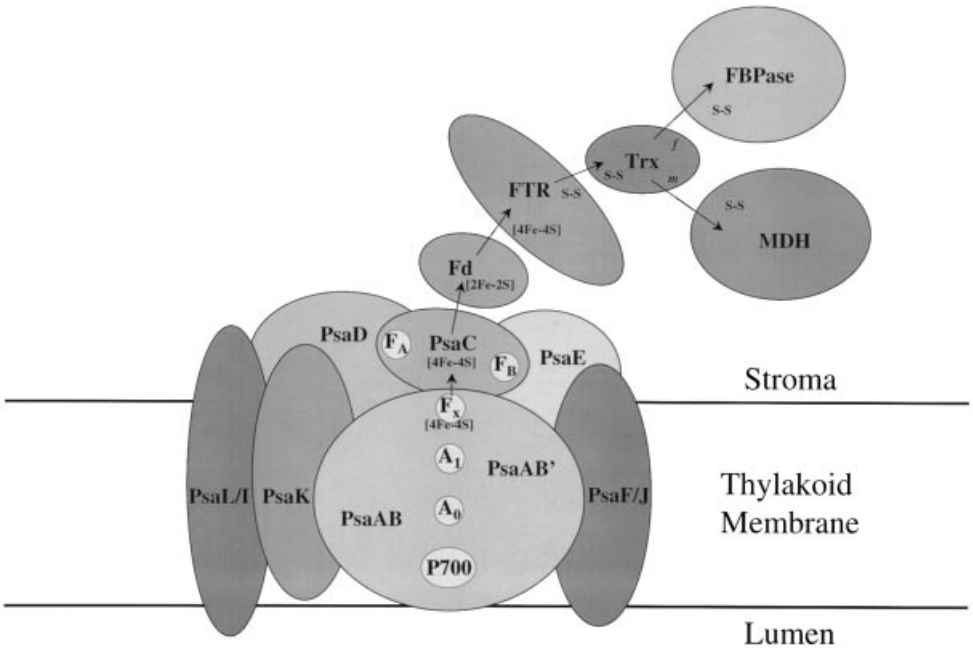

Fig. 2. Photosystem I produces reducing equivalents in the form of ferredoxin which is sensed by the FTR system to perform enzyme activation. Upon illumination, the electron emitted from the excited P700* near the lumenal side of the thylakoid membrane is transferred across the membrane to the [4Fe–4S] clusters of PsaC on the stromal side. The [4Fe–4S] clusters in turn reduce the [2Fe–2S] cluster of soluble ferredoxin. FTR transduces the reducing power of ferredoxin into reductive thiols for the activation of target enzymes via thioredoxin.

ferredoxins from photosynthetic organisms are known (Table 1) and the structure of the key electron/thiol transducer enzyme, FTR, has recently been determined (Dai *et al*. 2000). The structure of FTR and its functional implications are the central subjects of this review and interacting ferredoxin and thioredoxins are discussed in relation to this structure. A cyanobacterial and an algal thioredoxin structure have been available for some time. Recently the three-dimensional structures of spinach thioredoxin *f* and thioredoxin *m* have also been determined (Capitani *et al*. 2000).

The two most well-studied target enzymes of the ferredoxin/thioredoxin system, chloroplast FBPase and chloroplast MDH, have recently been analyzed by X-ray crystallography (Villeret *et al*. 1995a; Johansson *et al*. 1999; Carr *et al*. 1999; Chiadmi *et al*. 1999) and provide the first insight into the molecular background for the reductive activation. In chloroplast MDH the reducible disulfides have been located and a plausible mechanism for its activation has been proposed (Johansson *et al*. 1999; Carr *et al*. 1999). In spinach chloroplast FBPase no disulfides were visible in the electron density maps (Villeret *et al*. 1995a) but the recent structure of the pea enzyme clearly locates the regulatory disulfides and explains their function (Chiadmi *et al*. 1999). All these structures now provide a comprehensive view of how light regulates the activity of chloroplast enzymes through a chain of redox reactions.

2. Ferredoxin reduction by photosystem I

In oxygenic photosynthesis of cyanobacteria and plants, photosystem I (PSI) is one of the two pigment containing reaction centers located in the thylakoid membrane (Barber & Andersson, 1994). Upon illumination, the electron emitted from the excited P700* near the lumenal side of the thylakoid membrane is transferred across the membrane to the [4Fe–4S] clusters of PsaC on the stromal side. The [4Fe–4S] clusters in turn reduce the [2Fe–2S] cluster of soluble ferredoxin (Fig. 2). Cyanobacterial PSI consists of 11 protein subunits and 90 chlorophyll molecules (Krauss *et al*. 1996) (Fig. 3). PsaA and PsaB are the core of PSI and bind the electron transfer components P700, A0, A1, FX, β-carotene molecules and most of the chlorophylls. The other nine subunits are PsaC, PsaD, PsaE, PsaF, PsaI, PsaJ, PsaK, PsaL and PsaM. Except for PsaC, PsaD and PsaE, which are on the stromal side, all subunits are within the membrane.

Only PsaC, PsaA, and PsaB bind cofactors of the electron transfer systems. PsaC contains two [4Fe–4S] clusters, the FA and FB centers, which are the terminal electron acceptors in the electron transfer chain in PSI. PsaD helps PsaC to form a stable complex with the PsaA and PsaB core. PsaD and PsaE play an important role in the interaction between PsaC and soluble ferredoxins, which is crucial for the subsequent electron transfer to ferredoxin : $NADP^+$ reductase (FNR) and FTR.

After being reduced by PsaC, ferredoxins can function as general soluble electron donors in the stroma, which initialize a number of important biological processes (Knaff, 1996). The well-known function is the transfer of electrons to $NADP^+$ through FNR. NADPH then provides the reducing power for the synthesis of carbohydrates.

Recently a more detailed structural model of the stromal subunits PsaC, PsaD, and PsaE of PSI was obtained (Klukas *et al*. 1999a). The NMR structure of the subunit PsaE of PSI from *Synechococcus* sp. PCC7002 (Falzone *et al*. 1994) was used as a model to interpret the region of the electron density map corresponding to this subunit. Together, these subunits form a stromal ridge that extends ~ 30 Å beyond the membrane-integral regions. PsaE is located adjacent to PsaC. Together with some loops from membrane-integral subunits, the three stromal subunits form a wide cavity, the docking site for ferredoxin or flavodoxin (Lelong *et al*. 1996; Muhlenhoff *et al*. 1996).

Superimposing the NMR and X-ray model structures of the subunit PsaE reveals both to be almost identical in the core region (Klukas *et al*. 1999b). A long loop, described as flexible in the NMR study (Falzone *et al*. 1994), adopts a twisted conformation in the X-ray structure of PSI directed away from the PsaE core in a finger-like manner. Within the PSI complex, the N- and C-termini of PsaE face the stroma and are directed toward the outer rim of the PSI trimer. The β-strands B and C form part of the ferredoxin binding site (Klukas *et al*. 1999a). It is therefore likely that some amino acids of these strands interact with the water-soluble electron acceptors. The mutation of Arg39 to Gln(R39Q) at the C-terminus of the strand C is known to partly inhibit ferredoxin reduction (Sétif *et al*. 1995).

A mutant of *Synechocystis* PCC 6803, deficient in PsaE, assembles PSI reaction centers without the PsaE subunit (van Thor *et al*. 1999). Under conditions of acceptor-side rate-limited photoreduction assays *in vitro*, using FNR and either *Synechocystis* flavodoxin or spinach ferredoxin, lower rates of $NADP^+$ photoreduction were measured when PsaE-deficient membranes were used, as compared to the wild type. This effect of the PsaE mutation proved to be due to a decrease of the apparent affinity of the photoreduction assay system for the reductase. In the PsaE mutant, the relative FNR expression level was found

to be significantly increased, providing a possible explanation for the lack of a phenotype (i.e. a decrease in growth rate) that was expected from the lower rate of linear electron transport in the mutant. A PsaE-dependent transient ternary complex PSI/ferredoxin/FNR has been proposed to be formed during linear electron transport (van Thor *et al*. 1999).

3. Ferredoxins

Ferredoxins are distributed over a wide range of living organisms and can adopt different architectures in divergent organisms. Ferredoxins are the most extensively studied iron–sulfur proteins and have also served as prototypes for various iron–sulfur clusters, mainly the simple ones. Ferredoxins can be classified by the bonding of the iron–sulfur clusters into two types, the plant-type ferredoxins and the bacterial ferredoxins (Bruschi & Guerlesquin, 1988). Plant-type ferredoxins possess single [2Fe–2S] clusters, which are attached to the protein by four cysteine ligands. Bacterial-type ferredoxins have many variants which differ in the type ([3Fe–4S] or [4Fe–4S]) and the number of clusters.

Plant ferredoxins have a [2Fe–2S] cluster which operates at low redox potentials, typically −400 mV. The crystal structure of the first protein containing a plant-type [2Fe–2S] cluster was solved for a blue-green algal ferredoxin from *Spirulina platensis* (Fukuyama *et al*. 1980, 1995). Several three-dimensional structures of plant-type ferredoxins are now available (Table 1). All these ferredoxins share the same fold with a five-stranded β-sheet, two–three α-helices and a long loop containing three or four cysteine ligands to the iron atoms (Fig. 4). The β-strands form a mixed sheet, two pairs of antiparallel two-stranded sheets joined by a rather complicated crossover connection. All plant-type ferredoxins possess a fully conserved cluster-binding sequence motif $CX_4CX_2CX_{22-33}C$. The iron–sulfur clusters of all are located towards the outer edge of the molecule in the loop. The two irons are tetrahedrally coordinated by inorganic sulfide ions and cysteine residues.

4. Ferredoxin:thioredoxin reductase

FTR, which transduces the general redox signal from ferredoxin to thioredoxins, is a unique enzyme, completely different from the bacterial, plant and mammalian thioredoxin reductases which are flavoproteins reduced by NADPH (Williams, 1992; Jacquot *et al*. 1997; Dai *et al*. 1996). FTR is an iron–sulfur protein with a redox-active disulfide bridge that utilizes the [4Fe–4S] cluster to mediate electron transfer from the one-electron donor, the $[2Fe–2S]^{2+}$ cluster of ferredoxin, to the two-electron acceptor, the disulfide bridge of thioredoxin. Reduced thioredoxin then transfers the electrons to target enzymes via thiol/disulfide interchange reactions. FTR is a versatile enzyme in terms of reactivity. It reduces the chloroplastic *f*- and *m*-type thioredoxins (Trx-*f* and Trx-*m*) and *in vitro* also cytoplasmic thioredoxin *h* or *E. coli* thioredoxin very efficiently (Jacquot *et al*. 1997). This is in contrast to the plant NADPH-dependent thioredoxin reductase, a flavoenzyme which shows a higher specificity toward thioredoxins (Jacquot *et al*. 1997).

FTR is an αβ-heterodimer composed of a 13 kDa catalytic β-subunit with conserved sequence between species and a variable α-subunit of similar or smaller size. The β-subunit contains a redox active disulfide and a [4Fe–4S]-center. Most biochemical investigations have

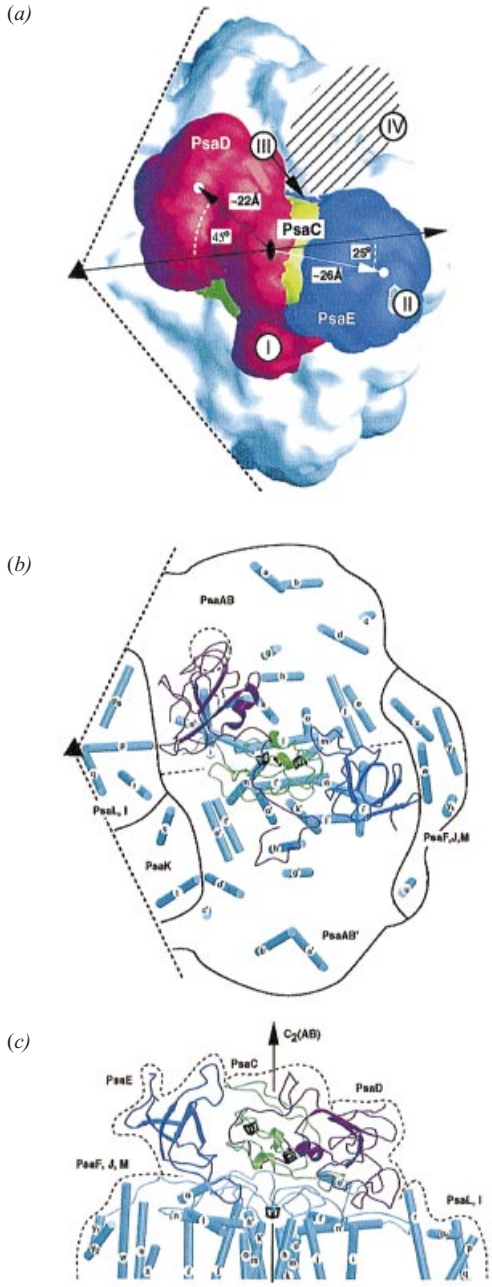

Fig. 3. The stromal ridge of PSI shown from the stromal side onto the membrane plane. (*a*) Simulated surface of the stromal ridge. PsaC is depicted in yellow, PsaD in red, PsaE in blue, and membrane-integral subunits in white. The approximate centers of mass of subunits PsaD and PsaE are indicated by white dots; for PsaC, it coincides with the symbol of the local 2-fold axis C2(AB). I, terminal extension of PsaD. It functions as a clasp for PsaC and is in close contact with PsaE. II, crystal contact surface of PsaE with the next trimer in the crystal lattice. III, loop CD of PsaE below PsaC. IV, binding site for ferredoxin/flavodoxin. (*b*) The equivalent view as in a showing the observed secondary structure elements of PSI. The α-helices of the membrane-integral parts are drawn as cylinders and shaded gray. The stromal subunits PsaC, PsaD, and PsaE are depicted as coil models showing their secondary structure elements. In addition, a large loop region of PsaD involved in the contact between this subunit

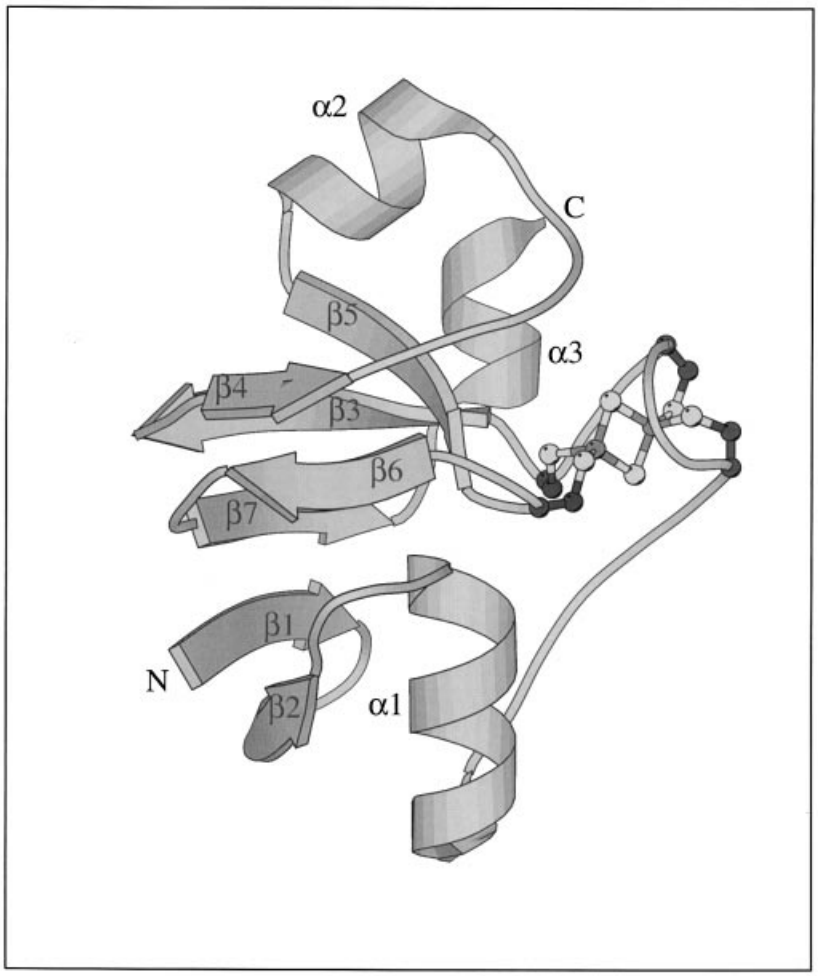

Fig. 4. Ferredoxin structure. Ferredoxins from photosynthetic organisms have very similar structures. The structure of ferredoxin from the green alga *Chlorella fusca* (pdb code: 1awd) contains three α-helices, a five-stranded β-sheet, two short stands and a long loop containing four cysteine ligands to the iron atoms of the [2Fe–2S] cluster (Bes *et al*. 1999).

been done on the spinach enzyme, for which a careful analysis of the iron–sulfur center has been performed (Staples *et al*. 1996, 1998). The three-dimensional structure has been determined for the cyanobacterial FTR from *Synechocystis* sp. PCC6803. This FTR shows no functional difference to the spinach enzyme but it is significantly more stable and can be obtained in larger amounts (Schwendtmayer *et al*. 1998).

---

and the core of PSI is marked. (*c*) Model of the stromal ridge of PSI showing the secondary structure elements. The view is into the ferredoxin/flavodoxin binding pocket with the trimeric axis on the right. The stromal subunits PsaC, -D, and -E as well as the iron–sulfur cluster FX are rendered in black. The protein backbone of the membrane-integral subunits (α-helices depicted as cylinders) are colored in gray. (Reprinted from Klukas *et al*. 1999a, with permission of the authors.)

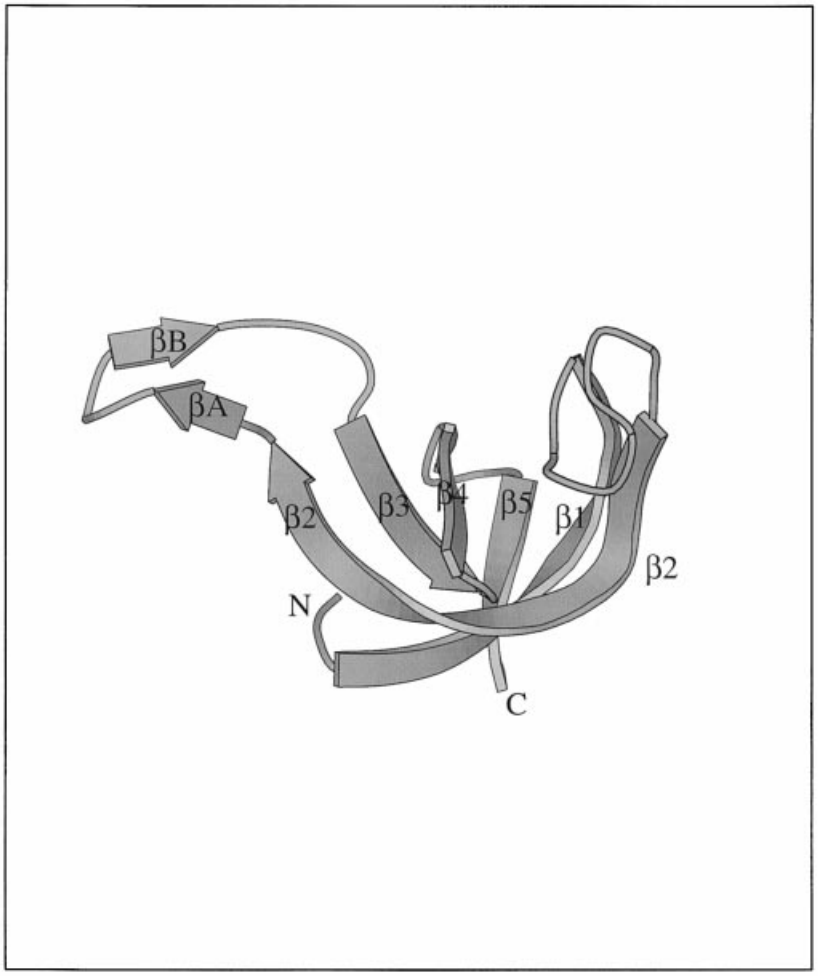

Fig. 5. Variable FTR subunit structure. A five stranded β-barrel forms the main body of the variable FTR subunit with two loops forming the upper, outer parts. One loop contains the short β-strands, βA annd βB.

4.1. Spectroscopic investigations of FTR

FTR has been analyzed by various spectroscopic techniques, like UV/visible, variable temperature magnetic circular dichroism (VTMCD), EPR, ENDOR and resonance Raman spectroscopy, to characterize its Fe–S cluster and to approach the reaction mechanism. Purified FTRs contain four non-heme iron atoms and four acid-labile sulfides per molecule as well as a redox active disulfide bridge (Droux *et al*. 1987). The UV/visible absorption spectra exhibit a protein band at 278 nm, a shoulder at 315 nm, and a broad peak centered around 410 nm (Schürmann, 1981; Droux *et al*. 1987; Schürmann & Gardet-Salvi, 1993; Staples *et al*. 1996). Depending on the source pure FTRs show a 278/410 nm absorbance ratio of 0·37 to 0·44. The UV/visible and CD spectra (Droux *et al*. 1987; Schürmann & Gardet-Salvi, 1993; Hirasawa *et al*. 1988) coupled with the absence of an EPR signal, are consistent with the presence of an $S = 0$ $[4Fe–4S]^{2+}$ cluster. This cluster exhibits very peculiar redox properties. It is redox-inactive over the potential range of -650 mV to at least $+300$ mV.

Attempts to reduce the cluster using dithionite, dithionite/DTT, dithionite/methyl viologen, and deazaflavin-mediated photoreduction produced no evidence of a paramagnetic ($S = 1/2$ or 3/2) $[4Fe–4S]^{+}$ cluster, which lead to the conclusion that the midpoint potential for the $[4Fe–4S]^{2+/+}$ couple must be < -650 mV (Staples *et al*. 1996).

Likewise it is very difficult to oxidize the iron–sulfur center to the $[4Fe–4S]^{3+}$ state. EPR signals were reported at low temperatures (< 30 K) for samples treated with ferricyanide (De La Torre *et al*. 1982) and they were interpreted in terms of oxidation to an $S = 1/2$ $[4Fe–4S]^{3+}$ state as found in oxidized high-potential iron–sulfur proteins (HiPIPs). This redox process had an estimated redox potential of above $+400$ mV in *N. muscorum* (De La Torre *et al*. 1982) and in spinach (Staples *et al*. 1996). Direct electrochemical measurements attributed a one-electron process with a midpoint potential of $+340$ mV to the $[4Fe–4S]^{3+/2+}$ couple (Salamon *et al*. 1995).

Considering the redox potentials of the disulfides in FTR and thioredoxins, which are in the range of -300 mV (Hirasawa *et al*. 1999), it is unlikely that this cluster is involved in mediating electron transfer from ferredoxin to the active site disulfide. A different function has been proposed based on experiments with a chemically modified FTR. Alkylation of one of the active-site cysteines with N-ethylmaleimide (NEM) resulted in spectroscopic signals which were assigned to a $[4Fe–4S]^{3+}$ cluster, however with properties quite different from an $S = 1/2$ $[4Fe–4S]^{3+}$ cluster in HiPIPs (Staples *et al*. 1996). Similar spectroscopic results were obtained when native FTR was reduced by a stoichiometric amount of reduced benzylviologen or transiently during the enzymatic turnover in presence of reductant and Trx-*f*. These observations confirmed the hypothesis that NEM-FTR corresponds to a stabilized form of a one-electron-reduced FTR reaction intermediate (Staples *et al*. 1998). In this intermediate the cluster is covalently attached to a cysteine-based thiyl radical formed through one electron reduction of the disulfide bridge, which results in oxidation of the cluster to the $S = 1/2$ $[4Fe–4S]^{3+}$ state. Thus the cluster stabilizes the one-electron-reduced reaction intermediate.

4.2 The three-dimensional structure of FTR from the cyanobacterium *Synechocystis* sp. PCC6803

The three-dimensional structure of FTR was determined with multiple isomorphous replacement methods with the help of multiple anomalous diffraction data collected on the iron edge for the iron–sulfur center (Dai *et al*. 2000). The structure was refined at 1·6 Å resolution with an *R*-value of 0·23 ($R_{\text{free}} = 0{\cdot}27$) with good stereochemistry and with all residues in the most favorable region of the Ramachandran plot. All residues except the first five of the catalytic chain were in good electron density.

4.2.1 The variable subunit

The FTR variable subunit is an open β-barrel structure which contains five antiparallel strands with the topology $+1, +1, +1, -4$ according to the nomenclature by Richardson (1981) (Fig. 5). The two first long strands of the barrel contain some irregularities when they bend around the barrel (Table 2). The variable subunit is heart shaped with a β-barrel forming the main body and with two loops forming the upper, outer parts of the heart (Fig. 5). The loop between the first two strands of the barrel is formed by residues 17–24 and contains two β-turns at its tip. The second loop is formed by residues 40–51 between the second and third

Table 2. *Secondary structure elements*

Catalytic subunit		
α1	8–27	
α2	32–51	
α3	62–70	
α4	76–83	
α5	105–115	
Hydrogen bonds in sheet-like structures		
28N	O91	
28O	N91	
29N	O101	
29O	N99	
31N	O97	
53O	N74	
55N	O72	
β-turns		
70–73	TFWN	
85–88	CHCM	
92–95	TPDN	
95–99	NDFA	
Variable subunit		
β1	4–16	Residues 10–12 bulge out and have no hydrogen bonds
β2	26–39	The regular strand is interrupted by a β-turn
βA	40–42	
βB	45–47	
β3	52–57	
β4	61–65	
β5	69–73	
β-turns		
2–5	TFWN	
18–21	HPEH	
21–24	HKKT	
28–31	LQGM	
66–69	RPDE	

strand and contain a β-hairpin with strands βA and βB. This loop dominates the interaction area with the catalytic subunit. The connections between β3 and β4 and between β4 and β5 are tighter and point outward at the side of the heart.

The structure of the variable chain of FTR is remarkably similar to the PsaE protein which is a subunit on the stromal side of photosystem I (Falzone *et al*. 1994; Schubert *et al*. 1998). About two thirds of the variable chain can be superimposed with an r.m.s. fit of 1·30–1·45 Å for the two available cyanobacterial PsaE structures (Table 3). The strands of the barrel are very similar in FTR and the two PsaE structures while the loops differ (Fig. 6). The two long loops of FTR are missing in PsaE and instead the loop between strands 3 and 4 is long. However, the variable chain of maize and spinach FTR have nine or eight extra residues, respectively, at this point so a similar loop probably exists in these enzymes. There is low (less than 15%) sequence homology between FTR and PsaE. The conserved residues are dominated by glycines and internal hydrophobic amino acids and appear to be identical for structural reasons. The general similarity between the two proteins suggests that the variable FTR subunit and PsaE contain a common ferredoxin binding domain. However, this

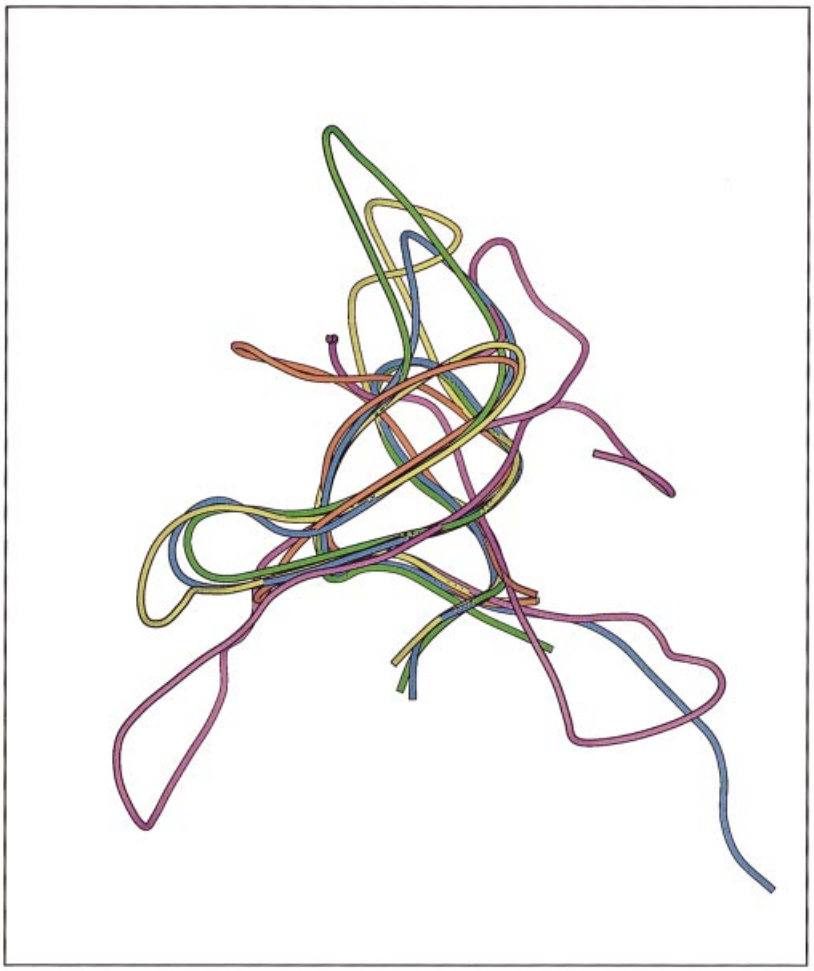

Fig. 6. Superposition of FTR and other structurally related proteins. Similar β-barrels form the common structure while loops between the strands vary. The figure shows simplified chain conformation of FTR (yellow) and PsaE from *Synechococcus* sp. (green) and from *Nostoc* sp. (blue), mouse SH3 domain from C-crk (pdb-code: 1cka) (Wu *et al*. 1995) (orange) and GroES type chaperone subunit Gp31 (pdb-code: 1g31) (Hunt *et al*. 1997) (magenta).

hypothesis is not supported by the way ferredoxin is supposed to bind to FTR (Dai *et al*. 2000; and see below).

FTR and PsaE are structurally similar to the SH3 domains (Fig. 6) and about half of the Cα-atoms of FTR superimpose closely on SH3 (Table 3). The peptide binding site of the SH3 domains corresponds in FTR to a part of the binding site for thioredoxin (Dai *et al*. 2000). The general shape of the variable chain is also similar to GroES (Fig. 6) and in this case again about half of the variable subunit of FTR can be closely superimposed (Table 3). To make the best superposition, the barrel has to be rotated around its axis such that the last strands of the GroES barrel superimpose on the first two strands of the variable FTR chain. There are no significant sequence similarities between the superimposed parts. The shape of the two molecules is similar and a long loop out from the tight barrel appears in a similar place in both

Table 3. *Superposition of the variable chain of FTR and structures of PsaE, SH3 and GroES using standard parameters in the lsq program in O (Jones, 1991) r.m.s. difference in Å*

Structure	PsaE	PsaE	SH3	GroES (Gp31)
r.m.s d. (Å)	1·45	1·30	1·43	1·61
Number of Cα	53	53	46	44
pdb code	1psf	1qp2	1cka	1g31

Superimposed residues in FTR and PsaE:

B1	MNVGDRVRVTSSVV	B14	B27	DLQGMEGEVAAVLT	B40
2	IERGSKVKILRKES	15	16	YWYGDVGTVASIDK	29
A2	VQRGSKVRILRPES	A15	A16	YWFQDVGTVASVDQ	A29
B48	SANLPVLVKFEQ	B59	B61	FKAHFRPDEVTLI	B73
31	GIIYPVIVRFNK	42	56	NTNNFAEHELEVV	68
A31	GIKYPVIVRFEK	A42	A56	NTNNFAEDELVEV	A68

Superimposed residues in FTR and SH3:

B4	GDRVRVTSSVV	B14	B28	LQGMEGEVAAVLT	B40
A134	AEYVRALFDFN	A144	A154	KKGDILRIRDKPE	A166
B52	PVLVKFEQRFKAHFRPDEVTLI		B73		
A169	WWNAEDSEGKRGMIPVPYVEKY		A190		

Superimposed residues in FTR and Gp31:

B4	GDRVRV	B9	B12	SVVV	B15	B30	GMEGEVAA	B37	B38	VLTG	B41		
C96	QKFVTC	C101	C105	AIPC	C108	C15	YVILVSEP	C21	C23	QAGD	C26		
B52	PVLVKFE	B58	B59	QRFKAHFRPDEVTLI	B73								
C46	PELCVVH	C52	C65	VGDLTSLPVGQIRNV	C79								

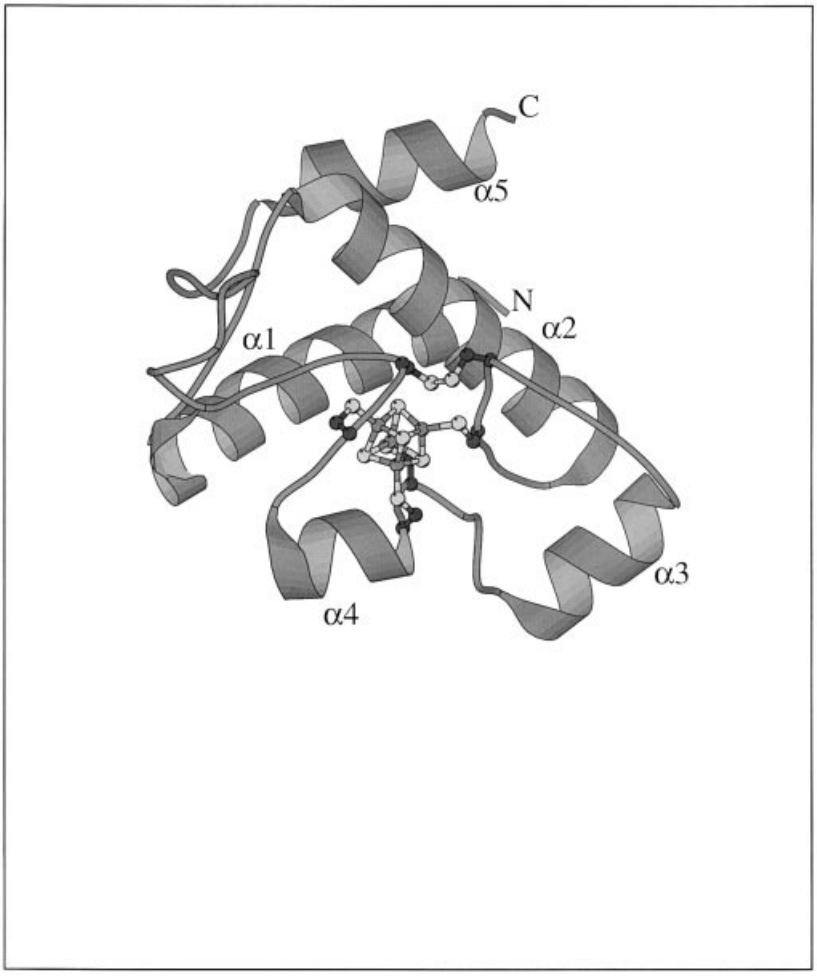

Fig. 7. Catalytic FTR subunit structure. The catalytic subunit has an overall α-helical structure containing five helices. The catalytic subunit contains the [4Fe–4S] cluster and the redox-active disulfide bridge.

structures. This loop between strands β2 and β3 of FTR forms the main interaction area with the catalytic chain of FTR. In GroES, the corresponding loop interacts with GroEL in the complex between the two (Xu *et al*. 1997).

4.2.2 The catalytic subunit

The catalytic subunit has essentially an overall α-helical structure containing five helices (Fig. 7). The subunit contains only very short strands with few hydrogen bonds and no real sheet is formed. The N-terminal half of the subunit, together with the C-terminal helix, forms an α-helical cap on top of the iron–sulfur center while the intervening 40 residues contain all the iron ligands and redox active cysteines. This part contains two additional short helices and intervening loops. Two sheet-like stretches of very short strands exist. One of these is close to the iron center with two hydrogen bonds between residues 53–55 and residues 72–74 in an antiparallel fashion. The second small sheet has the strand 28–31 in its center with two

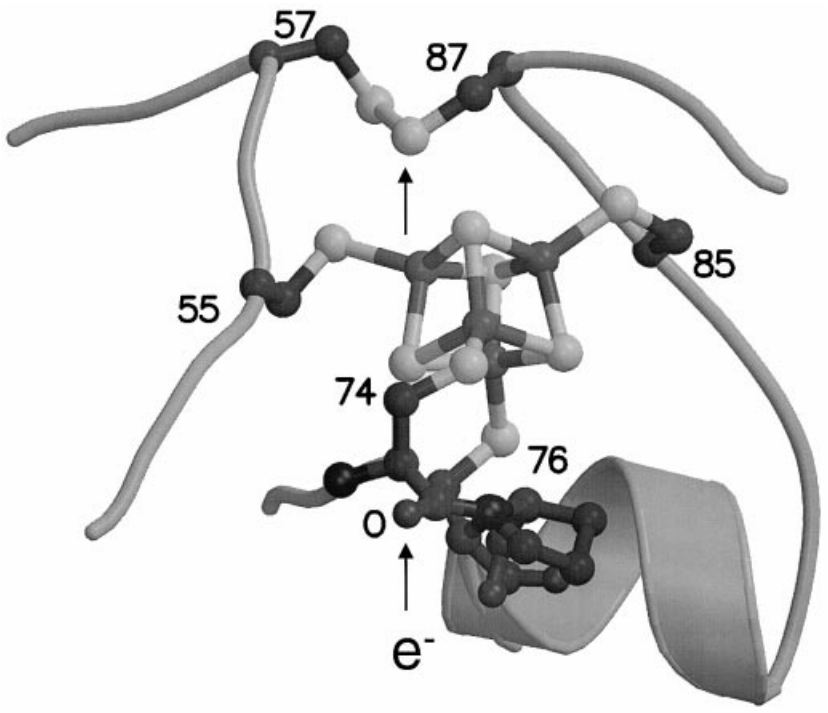

Fig. 8. The active site of FTR. The irons of the iron–sulfur center are coordinated by cysteines 55, 74, 76 and 85 in a normal cubane type geometry. The active site disulfide bridge between residues 57 and 87 is in van der Waals contact with the iron center, primarily the sulfur atom of Cys87. Beside the active site cysteines, Pro75 is also shown in ball and stick models and the oxygen atom in the *cis*-peptide bond between Cys74 and Pro75 is labeled. Incoming electrons can pass from ferredoxin to the main chain of Cys74 to the disulfide bridge via the iron center.

hydrogen bonds to residue 91, one hydrogen bond to residue 101 and two hydrogen bonds to residues 97–99. There are four β-turns in the catalytic domain, not including the first turn of α5 which is of 3_{10} type. Interestingly, one of these β-turns contains one of the iron-ligands and a cysteine of the active site disulfide. This structure may assist in stabilizing the close contact between Cys87 of the active disulfide and the iron center.

A search in the protein data bank for domains similar to the catalytic domain of FTR using the program TOP (Lu, 2000) revealed that there is no obviously similar structure known. Several high-scoring proteins only have the similarity that they are α-helical domains but without similar topology.

4.2.3 The iron–sulfur center and active site disulfide bridge

The iron–sulfur center and active site disulfide bridge are both located in the catalytic subunit. The irons of the iron–sulfur center (Fig. 8) are coordinated by cysteines 55, 74, 76 and 85 in a normal cubane type geometry (Howard & Rees, 1991; Beinert *et al*. 1997; Stout *et al*. 1998). The positions of the atoms in the cluster deviate by an r.m.s. of 0·05 Å from the atoms of the superimposed [4Fe–4S] cluster of *Azotobacter vinelandii* ferredoxin, pdb code 6fd1 (Stout *et al*. 1998). The cysteine sulfur atoms are hydrogen bonded to main chain nitrogen atoms as in other iron–sulfur proteins (Adman *et al*. 1975; Backes *et al*. 1991; Langen *et al*. 1992) except

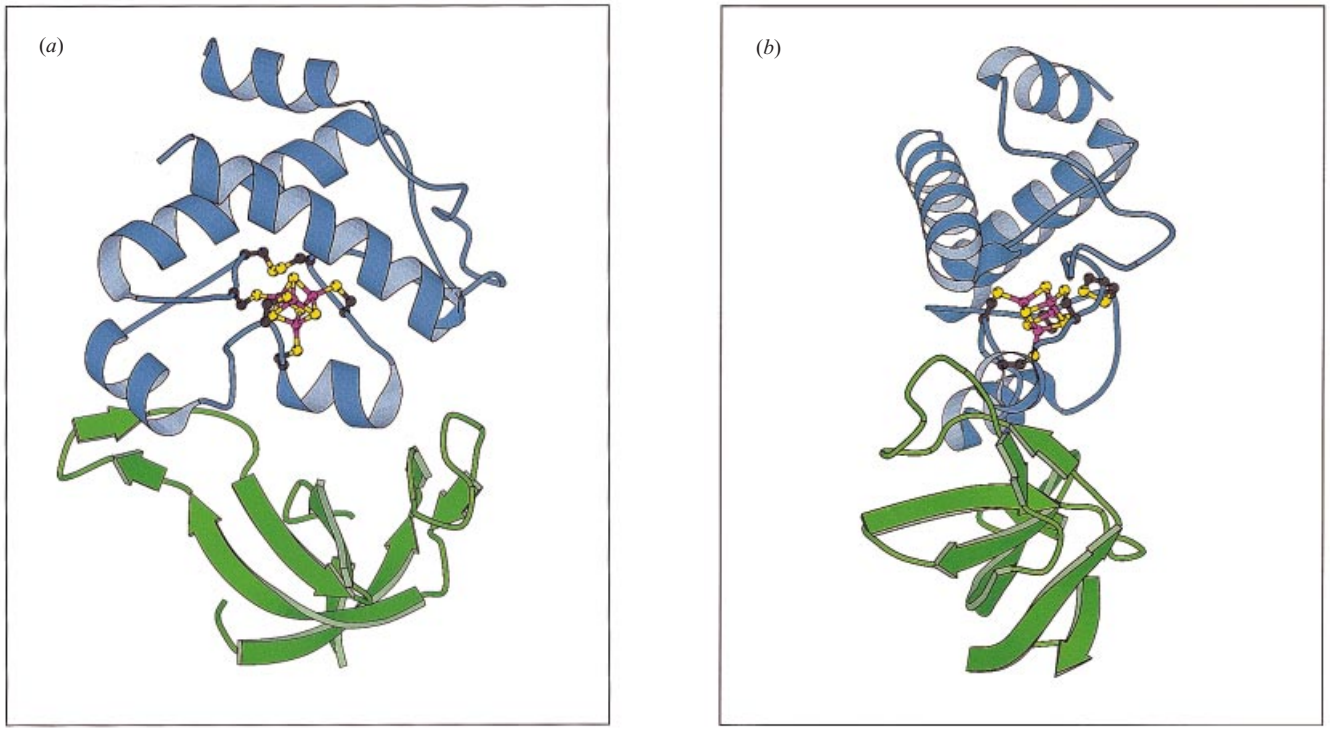

Fig. 9. The FTR heterodimer. (*a*) The catalytic subunit (blue) has an overall α-helical structure with loops between the helices containing the iron–sulfur ligands and redox active cysteines. The variable subunit (green) is heart shaped with the β-barrel forming the main body and with two loops forming the upper, outer parts of the heart. (*b*) FTR is an unusually thin molecule, a concave disk with dimensions 40 × 50 Å but only 10 Å across the center of the molecule where the iron–sulfur cluster is located.

Table 4. *Hydrogen bonds to cysteine sulphur atoms of the* [*Fe–4S*] *cluster*

Cysteine	Hydrogen donor	Distance (Å)
55 SG	N57	3·7
74 SG	—	—
76 SG	N79	3·5
85 SG	N89	3·4
85 SG	N90	3·4

Cys74 which is without hydrogen bond. Cys 55 and 76 are hydrogen bonded to N57 and N79, respectively and Cys85 is hydrogen bonded to both N89 and N90 (Table 4). None of the sulfide ions make any favorable hydrogen bond to the protein. The iron center is surrounded exclusively by hydrophobic residues: Ala18, Val39, Leu43, Pro56, Trp72, Pro78, Met79, Leu89 and Phe90, all coming from the catalytic subunit.

FTR is a truly unique [4Fe–4S] protein and differs in several respects from other [4Fe–4S] proteins. The all-helical structure of the catalytic subunit of FTR distinguishes it from other [4Fe–4S] proteins except endonuclease III (Kuo *et al*. 1992). However, the topology is in this case totally different. The sequence fingerprint for FTRs also differ from other iron–sulfur proteins where the liganding cysteines are separated by at least two residues. Thus, FTR does not possess the CXXCXXC or CXXC motifs, which are normally seen in [4Fe–4S] proteins (Howard & Rees, 1991). Rather, all ligands are located in short sequence motifs CXC, which constitutes a unique arrangement with the fingerprint **C**PCX$_{16}$**CP****C**X$_8$**C**HC (cluster ligands in bold type). Both cysteines in the central CPC motif are ligands to the iron–sulfur center while in the other two motifs the liganding cysteines are connected to the redox active cysteines in one CPC and one CHC motif where the second cysteines in these motifs are forming the disulfide bridge. His 86 in the latter motif is very close to the disulfide bridge and might increase the nucleophilicity of the active site cysteine Cys57.

The disulfide is composed of Cys57 and Cys87. Its geometry is left-handed in contrast to thioredoxins where it is right-handed. The torsion angles for the disulfide can be described as g$-$g$+$**g**g$+$g$+$ according to the nomenclature by Harrison & Sternberg (1996) and differ from the most common rotamer type, the symmetric left-handed spiral, only in the first torsion angle. The active site disulfide bridge is in van der Waals contact with the iron center, primarily the sulfur atom of Cys87 contacts the iron atom bound by Cys55 (Fig. 8). The sulfur atom of Cys87 is at 3·1 Å distance to the iron bound by Cys55 and to the sulfur atom of this cysteine. The closest sulfide ion of the cluster is 3·4 Å away from Cys87.

4.2.4 The dimer

The FTR heterodimer is an unusually thin molecule, a concave disk with dimensions 40×50 Å with only 10 Å across the center of the molecule where the iron–sulfur center is located (Fig. 9). The interactions between the catalytic and variable chains involve the very thin center of the molecule where only a small hydrophobic core is formed by residues Phe71, Trp72, Val77 and Pro78 of the catalytic chain with residues Ala49, Leu51 and His64 of the variable subunit. Instead, most of the interactions between the subunits occur between charged and polar residues forming hydrogen bonds (Table 5). Important interactions are made by Glu81 and Arg82 of the catalytic subunit which form both side chain to side chain

Table 5. *Interactions between variable and catalytic subunits*

Variable chain	Catalytic chain	Type of interaction
Tyr16	81–83	van der Waals
Tyr16 N	81 O	hydrogen bond
His17	**Glu81**	van der Waals
Trp42	65–69	van der Waals
47 N	**Glu66** OE2	hydrogen bond
Ala48	Phe71	van der Waals
Ser48	**Glu66** OE2	hydrogen bond
Leu51	71–72, 77–78	van der Waals
His64	Val77	van der Waals
His64 N	**Glu81** OE1	hydrogen bond
His64 ND1	**Glu81** OE2	hydrogen bond
His64 O	**Arg82** NH2	hydrogen bond
Glu69 OE1	**Arg82** NH2	hydrogen bond
Glu69 OE2	**Arg82** NH1	hydrogen bond

Residues in bold type are conserved within all species.

hydrogen bonds to His64 and Glu69 of the variable subunit, respectively, and hydrogen bonds to main chain atoms. Furthermore, the carbonyl oxygen of the main chain of Glu81 which is at the C-terminus of α4, forms a hydrogen bond to the main chain nitrogen of residue 16, which is in a β-sheet strand of the variable subunit. There are other side chain hydrogen bonds formed between Asp62 and Glu64 of the catalytic chain to Arg45 of the variable chain and side chain to main chain hydrogen bond formed between Glu66 of the catalytic chain and the main chain nitrogen of residue 48 in the variable chain. Besides this, there are van der Waals interactions involving, among others, Tyr16, His17 and Trp42 of the variable chain and Ala65, Glu81 and Lys83 of the catalytic chain.

4.3. Thioredoxin *f* and *m*

Thioredoxins are small ubiquitous redox proteins with a number of important cellular functions (for recent reviews see Holmgren, 1995; Powis *et al*. 1998; Åslund & Beckwith, 1999a,b). Thioredoxins are α/β-proteins which have a central five-stranded β-sheet surrounded by four helices with a redox-active disulfide at the N-terminus of α2 (Fig. 10).

Trx-*f* and Trx-*m* are the only two thioredoxins implicated in the ferredoxin:thioredoxin system. They have been distinguished by their target enzyme specificity. Trx-*f* displays a high specificity towards chloroplast FBPase and several other Calvin cycle enzymes whereas Trx-*m* interacts very efficiently with MDH, hence their names (Jacquot *et al*. 1997; Meyer *et al*. 1999; Schürmann & Jacquot 2000). The primary structures of the two chloroplast thioredoxins show relatively little resemblance with only 30% identities. Early studies demonstrated that spinach Trx-*m* is more similar to *E. coli* thioredoxin than Trx-*f*, both in sequence and in enzymatic specificity (Tsugita *et al*. 1983). Recent analyses of spinach Trx-*f* and Trx-*m* confirm at the structural level that Trx-*m* is closer to *E. coli* thioredoxin than Trx-*f* (Capitani *et al*. 2000). A major difference between Trx-*f* and Trx-*m* is the presence of a third cysteine, which is conserved in all Trx-*f*s. In the crystal structure, this Cys73 is exposed on the surface, 9·7 Å away from the accessible active-site Cys46. Mutagenesis studies show that this residue may participate in the interactions with the target enzyme (del Val *et al*. 1999).

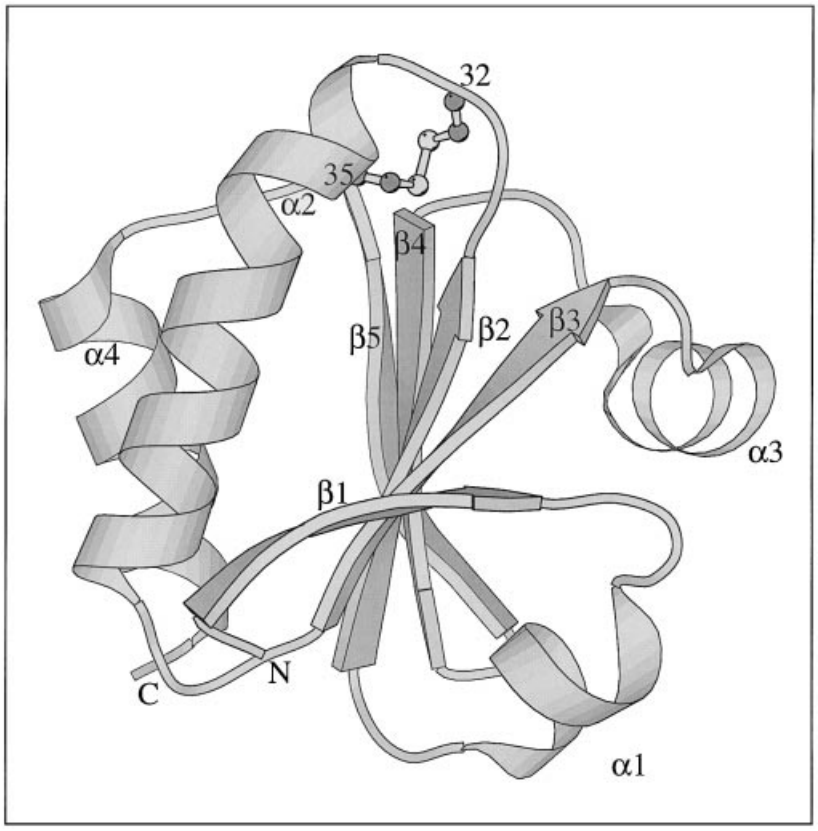

Fig. 10. Thioredoxin structure. Thioredoxins are α/β-proteins which have a central five-stranded β-sheet surrounded by four helices with redox-active disulfide between Cys32 and Cys35 at the N-terminus of α-2. The figure shows the structure of thioredoxin from *Anabaena* sp. 7120 (Saarinen *et al*. 1995).

In addition to the third cysteine, Trx-*f* has a substantially different distribution of polar, charged and hydrophobic residues around the active site with respect to *E. coli* thioredoxin of Trx-*m*. The active site of Trx-*f* is surrounded by a number of positive charges which may be instrumental in orienting Trx-*f* correctly when it interacts with its target proteins.

4.4 Ferredoxin and thioredoxin interactions

Thioredoxin catalyzed protein disulfide reductions have been shown to proceed through the formation of a heterodisulfide between the two reaction partners. There are strong indications for the formation of a mixed disulfide intermediate in the reduction of thioredoxin by FTR (Staples *et al*. 1996, 1998). This implies that during the state with the transient heterodisulfide, one side of the disk-shaped FTR-dimer is covered by the thioredoxin molecule. To complete the reduction of the disulfide, an additional electron has to be delivered to the iron center of the enzyme by a ferredoxin that docks on the opposite side of the FTR-dimer. The structure of the FTR-dimer suggests that both subunits together form the interaction surfaces for ferredoxin and thioredoxin (Fig. 11).

The surfaces on both sides of the molecule are highly conserved (see below). The disk has shape-complementarity to the ferredoxin molecule on one of its sides (Fig. 12). The potential

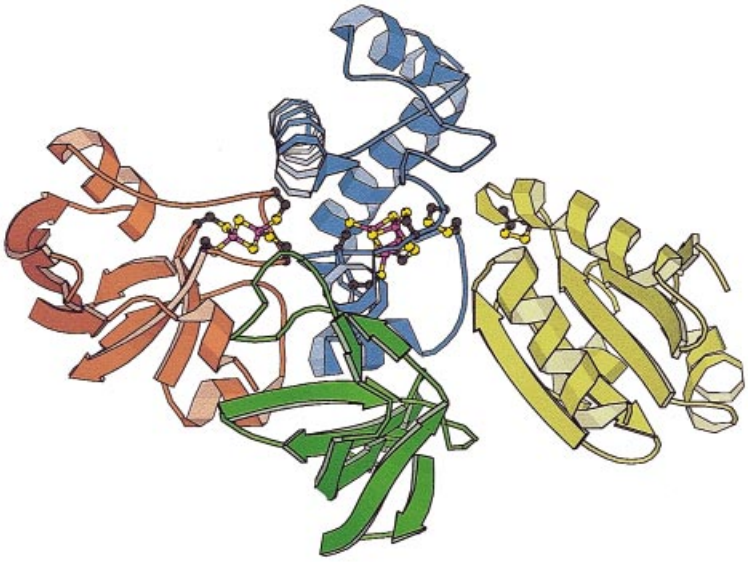

Fig. 11. Modelling of the electron transport chain from ferredoxin to thioredoxin. The disc-shaped structure of the FTR allows docking of a ferredoxin on one side of the molecule (red, to the left), while thioredoxin binds to the other side and forms a heterodisulfide with the enzyme (yellow, to the right). This intermediate can be reduced by an electron from a second ferredoxin molecule. The iron–sulfur centers and disulfide bridges are shown in ball and stick representation. Ferredoxins from *Anabaena* (Jacobson *et al*. 1993) and *Spirulina platensis* (Fukuyama *et al*. 1995) and thioredoxin from *Anabaena* sp. 7120 (Saarinen *et al*. 1995) were used in the docking studies.

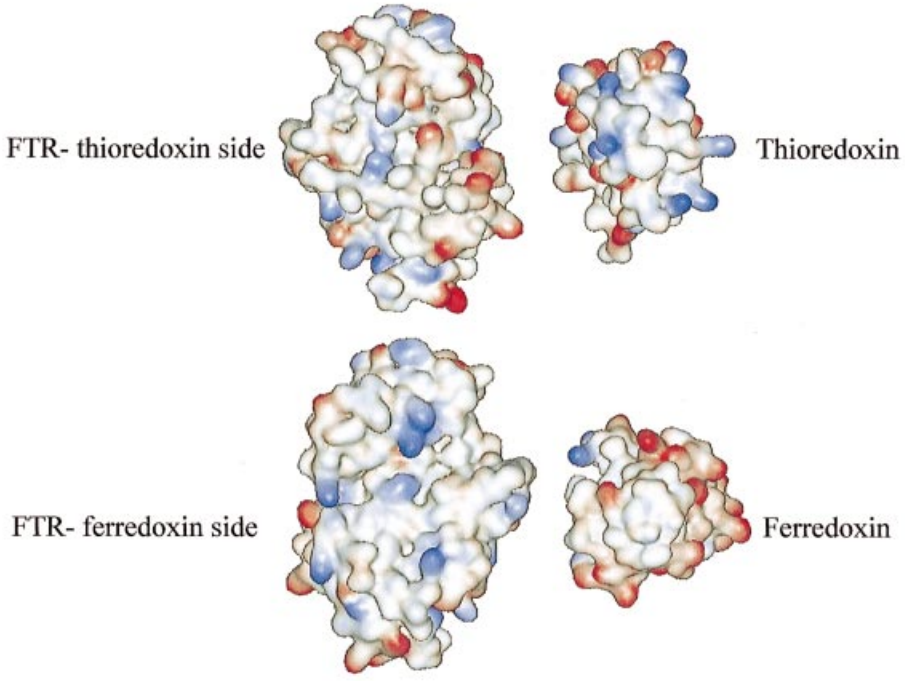

Fig. 12. Interaction surfaces of FTR and partners. Surface representation of the docking sites of FTR for thioredoxin and ferredoxin and the surfaces of thioredoxin and ferredoxin.

ferredoxin interaction area contains three positively charged residues at about 10 Å from the cluster. Together with hydrophobic residues around the Fe–S cluster they form a docking area for negatively charged ferredoxin. The ferredoxin interaction area is specific due to the presence of several charged residues. A clearly lower affinity between spinach ferredoxin and *Synechocystis* FTR was observed (Schwendtmayer *et al*. 1998) than what was reported for the homologous couple spinach ferredoxin and FTR (Hirasawa *et al*. 1998).

The thioredoxin interaction area is different and contains more hydrophobic residues and three histidines one of them very close to the active site. There is one negatively charged residue, Glu84, about 12 Å away from the FTR disulfide, which fits with a positively charged residue in thioredoxin. The absence of other charged groups makes the thioredoxin interaction area less specific which might be important since FTR reduces different thioredoxins present in the cell, as is the case in the spinach chloroplast. Even *Synechocystis* FTR is perfectly capable of reducing spinach Trx-*f*.

4.5 Mechanism of action

All known biological disulfide reductions except the one by FTR are catalyzed by flavoproteins or by thiol–disulfide exchange reactions (Williams, 1992). The unique property of the FTR iron–sulfur center to be able to cleave a disulfide does not appear to be due to an unusual geometry of the iron center since the iron sulfur cluster is very similar to other [4Fe–4S] clusters. The environment of the iron–sulfur cluster is not exceptional having, on average, one hydrogen bond per liganding cysteine and otherwise a surrounding hydrophobic environment. However, there is one unusual feature of the iron center: the close proximity to the active site disulfide bridge which appears to be the main reason for FTR's unique properties. Cys87 is so close to the iron sulfur center that it does not appear to exist as a free thiol until the final reduction step and, during previous steps, to interplay with the iron-sulfur center. Cys57, on the other hand, at the molecular surface of FTR should be the nucleophile attacking the thioredoxin disulfide in the first step of the reaction. His86 and Arg58 are very close to the disulfide bridge (3·9 and 5·6 Å, respectively) and might increase the nucleophilicity of the cysteine.

The reduction of a disulfide is a two-electron process while ferredoxin is a one-electron carrier. The initial electron from a ferredoxin molecule can be transferred via the iron–sulfur center directly to the disulfide that is in close contact with one iron atom of the cluster. Spectroscopic investigations have shown that the stable redox state of the [4Fe–4S] cluster is 2+. Reduction of the center to $[4Fe–4S]^{+}$ is extremely difficult (see above). Likewise, the oxidation to $[4Fe–4S]^{3+}$ is also not relevant at physiological conditions. This seems strange at first sight and indicates that no redox reaction involving the iron–sulfur cluster should occur at physiological conditions. The pioneering work of Staples *et al*. has explained the phenomenon by the formation of a one-electron reduced intermediate of the reaction. The one electron reduction of the protein results in an oxidation of the iron–sulfur cluster and a full reduction of the disulfide. Because of the redox-potentials of FTR, the one-electron reduction of FTR by ferredoxin results in an oxidation of the $[4Fe–4S]^{2+}$ cluster to an $[4Fe–4S]^{3+}$ cluster (Staples *et al*. 1996, 1998). In this step, one electron from the ferredoxin and one electron from the iron–sulfur cluster are used to cleave the disulfide bridge. In this intermediary state, labeling has shown that only one of the cysteines, Cys57, is a reactive thiol while the second cysteine is protected by the iron–sulfur cluster (Staples *et al*. 1996).

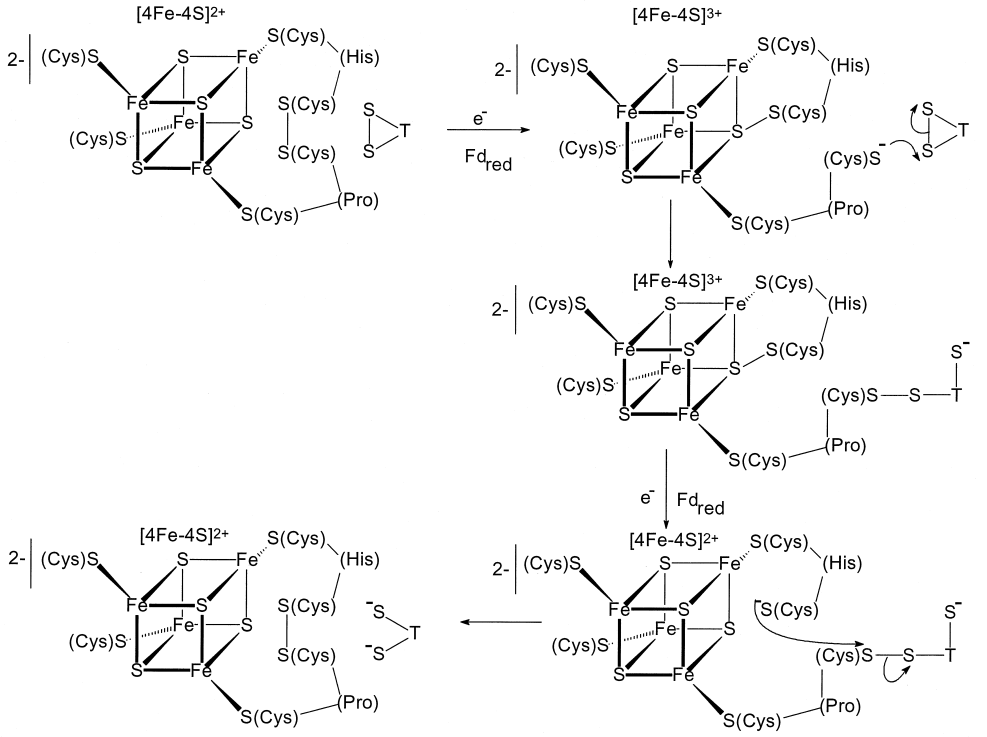

Fig. 13. Suggested mechanism of action (Staples *et al*. 1998). Cys87 is suggested to coordinate a sulfide ion of the iron–sulfur cluster in the intermediate stage. Reprinted with permission from Staples *et al*. (1998). Copyright 1998 American Chemical Society.

This intermediate stage has been suggested to have one of the redox-active cysteines, the buried cysteine Cys87, bound to the iron–sulfur cluster (Staples *et al*. 1998). Two possibilities for this intermediate were proposed; either a disulfide bridge formed to a sulfide ion in the cluster, or a five-coordinated iron where the fifth ligand should be Cys87. In the structure of FTR, Cys87 of the bridge is closest to one of the irons. Staples *et al*. (1998) favored this intermediate to be forming a disulfide with a sulfide ion (Fig. 13). The main argument for this is that in a chemical reaction, the sulfide ion should be a good nucleophile for the reaction. Such an intermediate is also supported by the existence of a Raman band (but was considered speculative in the absence of isotope measurements). The existence of a transient EPR signal is also taken to support such an intermediate since a similar signal is observed for the ferredoxin from *Azotobacter vinelandii* which has a cysteine close to the [4Fe–4S] cluster. However, as they note, no such cysteine–sulfide disulfide has been observed previously.

Dai *et al*. (2000) instead suggested that in the intermediate stage, Cys87 coordinates the iron. The tight interaction by Cys87 with one of the irons of the cluster in the FTR structure implicates that Cys87 coordinates the iron in a five-coordinated cluster (Fig. 14). As pointed out by Staples *et al*. (1998), there is some precedence for this type of penta-coordinated iron, because five-coordinated subsites of [4Fe–4S] clusters have been synthesized. These penta-coordinated iron clusters show modified redox potentials (Ciurli *et al*. 1990) analogous to those found for FTR (Staples *et al*. 1996, 1998). For the FTR intermediate the redox potential

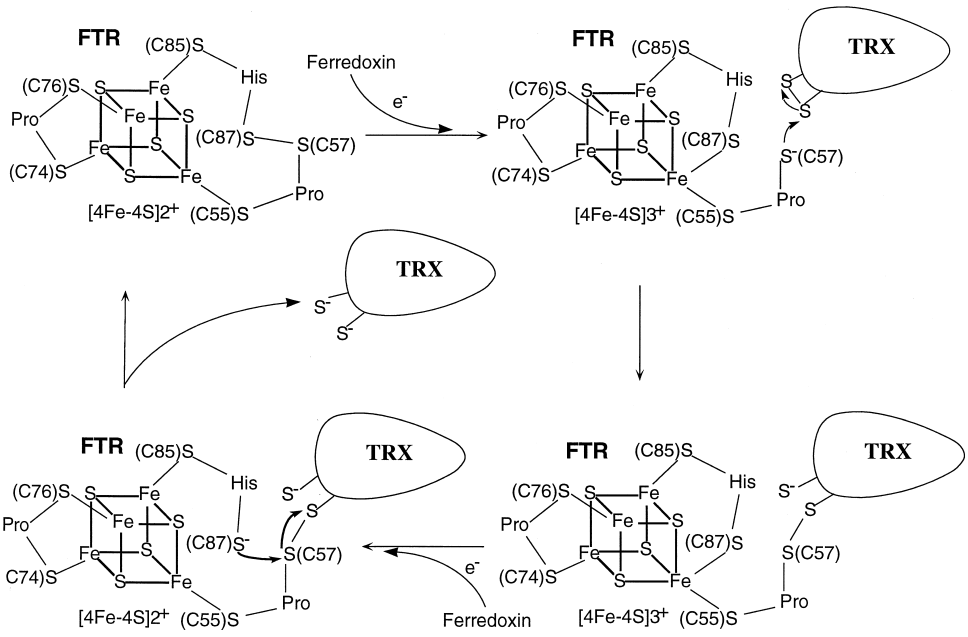

Fig. 14. Suggested mechanism of action (Dai *et al*. 2000) in which Cys87 with one of the irons of the cluster in the FTR structure implicates that Cys87 coordinates the iron in a five coordinated cluster.

of the $[4Fe–4S]^{3+,2+}$ couple is lowered from +420 mV to −210 mV, which is in the same region as the redox potential for the active-site disulfide (Salamon *et al*. 1995; Staples *et al*. 1998; Hirasawa *et al*. 1999). A similar lowering of redox potential by about 350–700 mV is observed for penta-coordinated iron clusters compared to tetra-coordinated iron clusters (Ciurli *et al*. 1990).

In analogy with known mechanisms, the reduction of thioredoxin has been proposed to proceed via a mixed disulfide between thioredoxin and FTR (Staples *et al*. 1996, 1998). The one-electron reduced intermediate, with its nucleophilic thiol Cys57, would be able to attack the disulfide bridge of thioredoxin to form a mixed disulfide. Such an intermediate complex would cover one of the sides of the flat FTR molecule and the second electron for the reduction should be delivered by the next incoming ferredoxin which has to dock on the opposite side of the flat disk-like heterodimer. The thin FTR molecule seems ideally suited for electron transfer between ferredoxin and thioredoxin. The shape of one side is complementary to ferredoxin and different ferredoxins could be docked to FTR. The iron–sulfur ligands on the ferredoxin side of the disk-formed FTR molecule are connected by Pro75 in a CPC motif. The main chain of this motif is exposed towards the ferredoxin side and docking of a ferredoxin to this site should give a short through-bond electron transfer route from the bound ferredoxin to the iron–sulfur center. The short distance through the enzyme from the ferredoxin docking site through the iron–sulfur center to the closely associated Cys87 of the active site disulfide seem ideally suited for its purpose.

The second electron delivered by a new ferredoxin molecule to the ferredoxin binding site reduces the iron–sulfur center back to its original 2+ oxidation state while Cys87 becomes a nucleophilic thiol that can attack the heterodisulfide bridge between FTR and thioredoxin

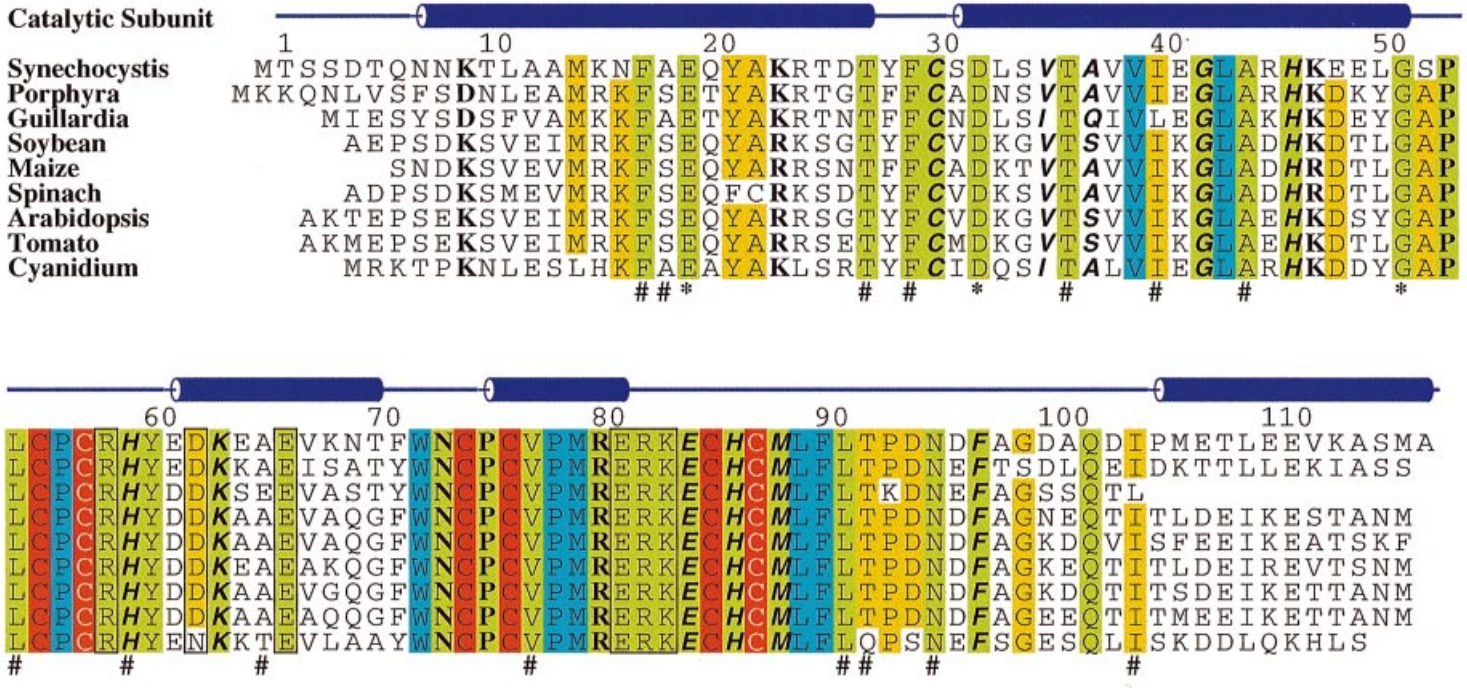

Fig. 15. FTR sequences; catalytic subunit. The sequences were aligned using CLUSTALX (Thompson *et al.* 1997). For *Arabidopsis* and tomato the N-terminus was determined by similarity. The sequences, retrieved from the Swiss Prot and the EMBL nucleotide data banks have the following accession numbers: *Arabidopsis* AC006955(AAD22336); Tomato AW041151; Soybean O49856; spinach P41348; Maize P41347; *Synechocystis* Q55389; *Porphyra* P51386; *Cyanidium* AF022186(AAF13004); *Guillardia* O78461, Iron coordinating cysteines are shown in red with black text, redox-active cysteines in red with white text. Residues surrounding the iron–sulfur center are colored blue. Beside these colors, completely conserved residues are in green and those which are the same in all but one sequence are in yellow. Residues on the thioredoxin and ferredoxin side are in bold while those residues which interact with the variable subunit are boxed. An asterisk * below the residue means that the residues probably are conserved for structural reasons and a # symbol represents internal residues. The location of helices are shown by cylinders on top of the alignment.

and thereby release the fully reduced thioredoxin. Such a mechanism is entirely compatible with the disk shaped structure of FTR, which would allow docking of a second ferredoxin molecule on one side of the molecule, while thioredoxin is bound to the other side via the intermolecular disulfide bridge (Fig. 11).

4.6 Comparison with other chloroplast FTRs

Sequences for the catalytic subunits of FTR are available from nine different species (Fig. 15) and for the variable subunit from six species (Fig. 16). For both spinach subunits a second gene sequence exists showing some minor differences. These second genes, however, might not be expressed since their sequences do not correspond to the ones of the isolated proteins.

The variable subunits show pronounced sequence diversity. There is also a striking difference between plant and cyanobacterial enzymes. The plant enzymes have extensions in the N-termina, but besides this, few differences exist in chain length in the variable chain. There is a two-residue deletion between the first two strands in the plant enzymes, while the loop between strands β3 and β4 is eight or nine residues longer. The long N-terminus in the spinach variable chain has been shown with truncation mutants *in vitro* (16 resp. 24 residues deleted) not to be important for catalysis (unpublished results). This is consistent with the position of the N-terminus in *Synechocystis* FTR on the side farthest away from the catalytic subunit. All conserved residues in the variable chain are either internal or glycines that are conserved for structural reasons and residues in the interaction area with the catalytic subunit (Table 6). Most of these interactions are formed by residues in the long loop between $\beta 2$ and $\beta 3$ but also involve a few residues at the ends of the other strands (Fig. 16). Among the conserved residues are those which make hydrogen bonds to the catalytic subunit.

The primary structures of the catalytic subunits are highly conserved between all species analyzed. All ligands to the iron–sulfur center and the surrounding hydrophobic residues are conserved as well as the active site cysteines. As for the variable subunit, several residues in the catalytic subunit which participate in subunit interactions are conserved (Table 6, Fig. 15). Furthermore, the surfaces on both sides of the molecule are highly conserved and should form the main interaction area with ferredoxin on one side and thioredoxin at the other. The ferredoxin interaction area contains three positively charged residues at about 10 Å from the cluster. They might be responsible for the correct orientation of the negatively charged ferredoxin when it is docking. Some hydrophobic residues around the Fe–S cluster might also be involved in the interaction. The thioredoxin interaction area is different and contains more hydrophobic residues and three histidines one of them very close to the active site. This histidine (His86) could increase the nucleophilicity of the thiol. There is one negatively charged residue not too far from the disulfide in FTR, Glu84 and about 12 Å away, which may fit with a positively charged residue in thioredoxin. This area also contains a conserved cysteine residue that might have some particular function.

The recent sequencing of the complete genome of the *archaea Archaeoglobus fulgidus* (Klenk *et al*. 1997) and *Methanobacterium thermoautotrophicum* (Smith *et al*. 1997) has revealed the presence of a protein with striking similarities to the catalytic subunit of FTR. Although there are few sequence identities with the known FTRs, the Fe–S binding motifs are essentially conserved suggesting that this protein also contains a [4Fe–4S] cluster next to a disulfide bridge and might be the ancestor of the catalytic subunit of the plant FTR.

Fig. 16. FTR sequences; variable chain. The sequences were aligned as those in Fig. 15. The N-terminus for the *Arabidopsis* and tomato subunits is not known. The sequences, retrieved from the Swiss Prot and the EMBL nucleotide data banks have the following accession numbers: *Arabidopsis* AB018110; Tomato AW092527; Maize P80680; spinach P38365; *Anacystis* P24018; *Synechocystis* Q55781. Completely conserved residues are in green and those that are the same in all but one sequence are in yellow. Boxed residues make interactions with the catalytic subunit. An asterisk * below the residue means that the residues probably are conserved for structural reasons and a # symbol represents internal residues. The location of β-strands in the barrel are shown by arrows on top of the alignment.

Table 6. *Conserved residues*

Catalytic subunit	
Met14	Facing the ferredoxin interaction side
Phe17	Internal
Glu19	Structural
Thr27	Internal
Phe29	Internal
Cys30	Facing the thioredoxin interaction side
Asp32	Structural
Val35	Facing the thioredoxin interaction side
Thr36	Internal
Val38	Facing the ferredoxin interaction side
Val39	Residue surrounding the iron–sulfur cluster
Ile40	Internal
Gly42	Facing the thioredoxin interaction side
Leu43	Iron–sulfur cluster surrounding
Ala44	Internal
His46	Facing the thioredoxin interaction side
Gly51	Structural
Pro53	Facing the ferredoxin interaction side
Leu54	Internal
Cys55	Iron ligand
Pro56	Iron–sulfur cluster surrounding
Cys57	Active site disulfide
Arg58	Subunit interaction
His59	Facing the thioredoxin interaction side
Tyr60	Internal
Asp62	Subunit interaction
Lys63	Facing the thioredoxin interaction side
Ala65	Internal
Glu66	Subunit interaction
Trp72	Iron–sulfur cluster surrounding
Asn73	Facing the ferredoxin interaction side
Cys74	Iron ligand
Pro75	Facing the ferredoxin interaction side
Cys76	Iron ligand
Val77	Internal
Pro78	Iron–sulfur cluster surrounding
Met79	Iron–sulfur cluster surrounding
Arg80	Facing the ferredoxin interaction side
Glu81	Subunit interaction
Arg82	Subunit interaction
Lys83	Subunit interaction
Glu84	Facing the thioredoxin interaction side
Cys85	Iron ligand
His86	Facing the thioredoxin interaction side
Cys87	Active site disulfide
Met88	Facing the thioredoxin interaction side
Leu89	Iron–sulfur cluster surrounding
Phe90	Iron–sulfur cluster surrounding
Leu91	Internal
Thr92	Internal
Pro93	
Asn95	Internal
Phe97	Facing the thioredoxin interaction side
Gln101	
Ile103	Internal
Glu111	

Table 6. (*Cont.*)

Variable subunit	
Gly4	Structural
Val7	Internal
Val9	Internal
Val14	Internal
Tyr16	Subunit interaction
His17	Subunit interaction
Gly33	
Trp42	Subunit interaction
Gly46	Structural
Asn50	Subunit interaction
Pro52	Internal
Val55	Internal
His64	Subunit interaction
Glu69	Subunit interaction

5. Target enzymes

A number of chloroplast enzymes have been shown to be light regulated (Table 7). However, in order to be activated through the ferredoxin:thioredoxin system, a regulatory disulfide, which can be reduced by thioredoxin, has to be present in the enzyme. For several target enzymes involved in the photosynthetic carbon assimilation the regulatory cysteines have been located in the primary structure and the principal activator thioredoxin determined (Table 7) (Schürmann & Buchanan 2000; Schürmann & Jacquot 2000). Until recently, no structural information was available for any target enzyme except for the spinach chloroplast FBPase (Villeret *et al*. 1995a). In this structure, however, the regulatory disulfide was not visible. Now the three-dimensional structures of oxidized NADP–MDH and pea FBPase, two of the most studied target enzymes, have been solved (Johansson *et al*. 1999; Carr *et al*. 1999; Chiadmi *et al*. 1999). With the knowledge of these crystal structures the structural basis for light activation is emerging and we are beginning to understand some of the processes occurring during the final activating steps of the redox cascade.

5.1 NADP-dependent malate dehydrogenase

NADP–MDH is found in the chloroplasts of C3 and C4 plants. In C3 plants, like spinach, this enzyme is not directly involved in carbon fixation, but functions in a shuttle mechanism exporting reducing equivalents in the form of malate from the chloroplast. In C4 plants the primary CO_2 fixation is spatially separated from the incorporation into carbohydrates by the Calvin cycle. CO_2 is first assimilated into oxaloacetate by phosphoenolpyruvate carboxylase. In certain of these plants, like maize or sorghum, the chloroplastic NADP–MDH is an essential enzyme in this carbon trapping and transport mechanism. It reduces oxaloacetate, the initial fixation product, to malate, which is then conveyed via plasmodesmata from the mesophyll into the bundle-sheath cells where it is decarboxylated by malic enzyme and the liberated CO_2 incorporated into sugars by the enzymes of the Calvin cycle (Hatch, 1987).

As this CO_2 trapping and concentrating mechanism is highly energy dependent, its strict control is very important for the plant. For the NADP–MDH, control is accomplished by

Table 7. *Target enzymes*

Target enzyme	Organism	Conserved regulatory cysteines	Means of activation	Reference
NADP–MDH	*Flaveria bidentis* *Sorghum vulgare*	–QKPE**C**FGVF**C**LTYD– –RKGE**C**FGVF**C**TTYD– 24 29 –AEKK**C**VAHLTGEGIAV**C**DLPEDTMLPGEM –AEKK**C**VAHLTGEGNAY**C**DVPEDTMLPGEV 365 377	Activated only by reduction of *both* disulfides by either Trx-*f* or Trx-*m*	Carr *et al*. 1999 Johansson *et al*. 1999
FBPase	Pea	–E**C**LPDFGDDSDDNTLGTEEQR**C**IVNVCQP– 153 173	Activated both by disulfide reduction (Trx-*f*) and/or changes in pH and $[Mg^{2+}]$	Chiadmi *et al*. 1999
PRK	Spinach	–SG**C**GKSTFMRRLTSVFGX$_{17}$SDTTTVI**C**LD 16 55	Activated by Trx-*f*	Porter *et al*. 1988 Brandes *et al*. 1996
CF_1-ATPase γ-subunit	Pea	–EI**C**DINGN**C**VD– 198 204	Activated by Trx-*f*	Schwarz *et al*. 1997
SBPase	Wheat	–AS**C**GGTA**C**VN– 52 57	Activated by Trx-*f*	Dunford *et al*. 1998
G6PDH	Potato	–**C**RIDKRED**C**– 149 157	Inactivated by Trx-*m*	Wenderoth *et al*. 1997
Rubisco activase	*Arabidopsis thaliana*	–EG**C**TDPVAENFDPTARSDDGT**C**VYNF 392 411	Activated by Trx-*f*	Zhang & Portis, 1999

reversible covalent modification of two redox active disulfide bridges through the ferredoxin/thioredoxin system.

In contrast to NAD-dependent MDHs, which are permanently active (Miginiac-Maslow *et al*. 1997), the NADP-dependent chloroplastic MDHs are regulated by light. The chloroplast enzyme is totally inactive in the dark and activated by light through the ferredoxin : thioredoxin system (Jacquot *et al*. 1997). Based on recent structural information (Johansson *et al*. 1999; Carr *et al*. 1999) we begin to understand the mechanism by which the inactive enzyme is converted to a fully active one.

The regulatory disulfide bridges are located in two terminal sequence extensions not present in the constitutively active NAD-dependent MDHs (Birktoft *et al*. 1989; Gleason *et al*. 1994; Chapman *et al*. 1999). The N-terminal extension is about 43 amino acid residues and contains two cysteines that form one of the disulfides. The C-terminal extension is about 13 residues and contains one cysteine, which makes a disulfide with a cysteine in the last helix in the MDH core, present in all MDHs. Both disulfides are on the surface of the protein and are easily accessible for thioredoxin reduction (Fig. 17). Both disulfides need to be reduced to get a totally active enzyme, however, the mechanism of inactivation is distinctly different for the two extensions. The N-terminal extension is sitting like a wedge between domains in the enzyme, thereby inhibiting necessary flexibility for catalysis to occur. The action of the C-terminal extension is of a more direct nature. The very C-terminus is reaching into the active site and acts like an internal inhibitor of the enzyme.

5.1.1 Regulatory role of the N-terminal extension

The reduction of the N-termini has been shown to be the rate-limiting step during activation. It was early hypothesized that a conformational change was occurring after reduction of the disulfide, possibly making the active site more flexible and position important residues more favorably for catalysis.

The N-terminal disulfide between cysteines 24 and 29 (sorghum numbering) is positioned approximately in the middle of the extension, which is located at the interface between subunits (Fig. 17). It is composed of two cysteines separated by four residues, a common motif for redox active disulfides. A number of, mainly hydrophobic, interactions are made between the extension to both the catalytic domain in one subunit and the coenzyme-binding domain in the other (Fig. 18). Based on the crystallographic studies, the N-terminal extension is highly flexible, a feature possibly necessary for the activation process. It is only a region of about 10 residues around the disulfide which is clearly defined, forming a short 3_{10} helix, thereby making a good docking target for the reduced thioredoxin.

When comparing the position of domains relative to each other in the dimer between NAD- and NADP-dependent MDHs, one can determine that there is a slight rotational movement, possibly caused by the wedge-like action of the extension, in such a way that the catalytic domain in one of the monomers is pushed away from the catalytically favorable position. The breaking of the N-terminal disulfide bridge would further increase the flexibility of the whole extension and possibly remove it from its wedged position between the domains. The reduction of the disulfide is thought to relax this rigid structure and free the catalytic domain to adopt its catalytic conformation.

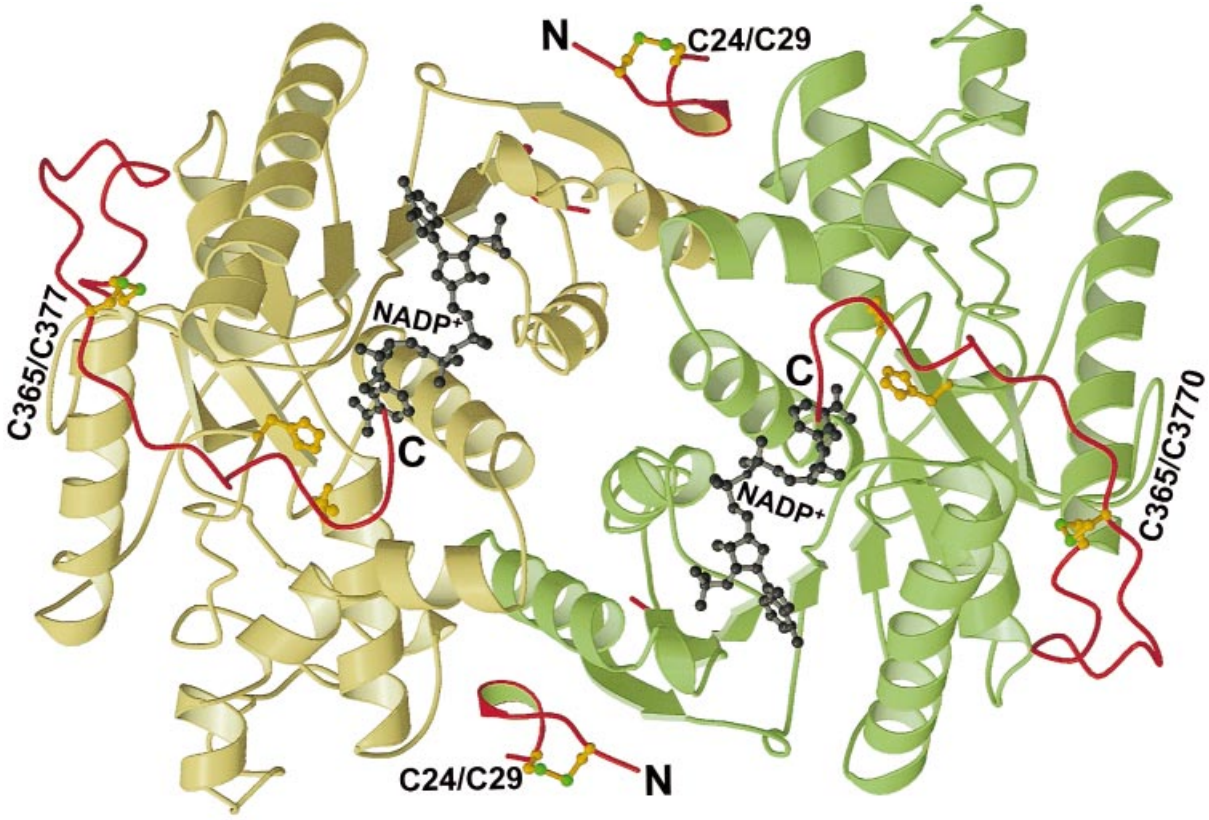

Fig. 17. The dimeric NADP-dependent MDH. The two subunits are in green and yellow. In red are the N- and C-terminal extensions, specific for all chloroplastic NADP-MDHs. In each of the extensions is one regulatory disulfide bridge present. In the N-terminal extension, this disulfide is comprised of Cys24 and Cys29. The N-terminal extensions are sitting like wedges between the subunits, thereby locking the domains relative to each other. The C-terminal extensions are folding back into the active sites and the disulfide between Cys365 and Cys377 stabilizes this conformation. The very C-termini are interacting with residues of the active site (Asp201 and His229, shown in gold) and with the $NADP^+$ (here modeled from the *T. flavus* NAD coordinates, pdb code: 1bmd).

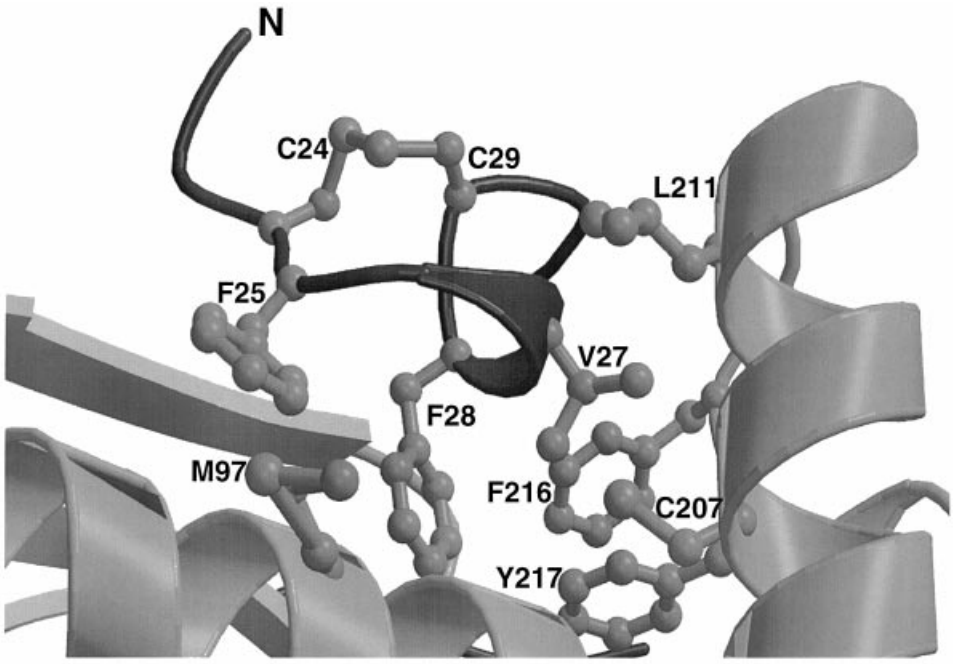

Fig. 18. Close-up on the interactions between the N-terminal extension and the rest of the enzyme. The extension containing the disulfide (C24/C29) is sitting like a wedge between the domains and interacts with the rest of the enzyme in a hydrophobic pocket. This results in the locking of the catalytic domain of one subunit with the coenzyme-binding domain of the other. Reduction of the disulfide would increase the flexibility, release the extension, and make the domains free to move relative to each other to adopt a conformation more favorable for catalysis. The regions both before and after the N-terminal disulfide are flexible and not seen in the crystal structure.

5.1.2 Regulatory role of the C-terminal extension

The position of the C-terminal disulfide between cysteines 365 and 377 is at the edge of the molecule where the extension after the last helix loops back and Cys377 in the extension makes a disulfide bond with Cys365 in the last stretch of that last helix (Fig. 17). There is a stretch of 11 residues separating the two cysteines involved in the disulfide.

When the C-terminal disulfide is oxidized, access to the active site is prevented, owing to the C-terminus shielding the entrance (Fig. 19). The inactivation by the extension is brought about by the C-terminus bending back into the active site where it occupies the position of the natural substrate oxaloacetate. This mode of action where a part of the molecule is mimicking the natural substrate by binding to its own active site has been termed ‘intrasteric inhibition’. This has earlier been seen in protein kinases where the self-inhibition is effected by a stretch of amino acids, which mimics the consensus sequence of the substrate. Mutational studies have shown that the negative charges of the last residues are of importance for this mode of action. When mutating the penultimate glutamate into a glutamine or deleting the last two residues, in combination with elimination of the N-terminal disulfide, a fully active enzyme is obtained with no need for thioredoxin activation, but with a lower affinity for oxaloacetate. This suggests that the C-terminus is somehow restricting access to the active site, thus supporting the hypothesis that the carboxyl groups of the C-terminus are mimicking the substrate, which also has two carboxyl groups.

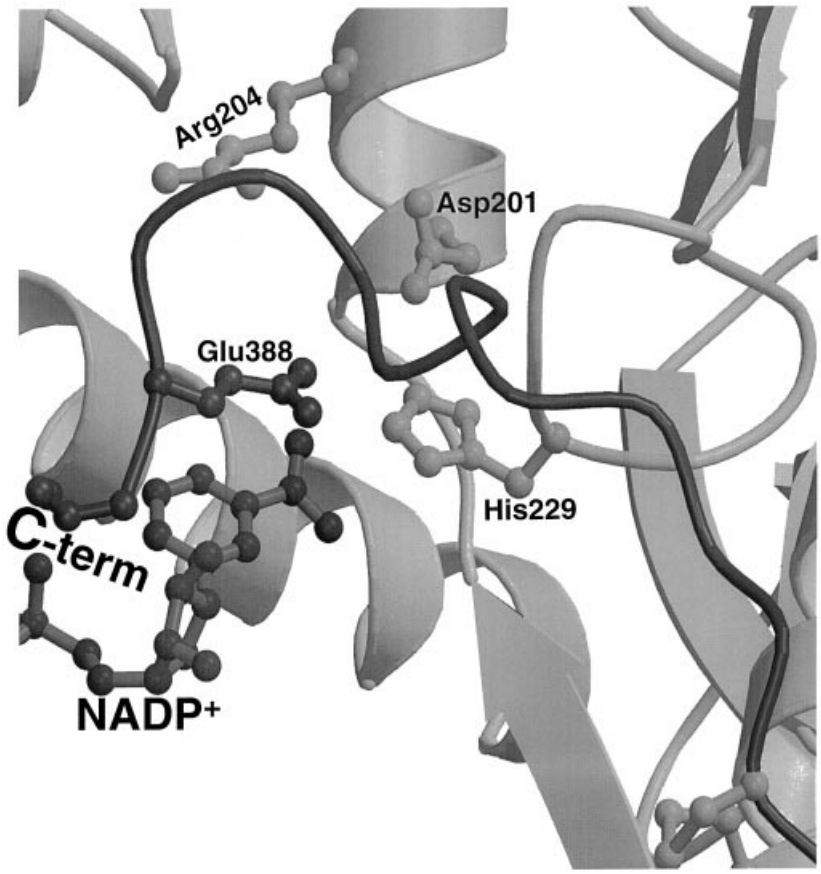

Fig. 19. Close-up view of the active site of NADP-MDH. The C-terminal extension loops back from the disulfide (at the bottom right corner) into the active site. The penultimate residue is the negatively charged Glu388, which is interacting with the active site His229 by two hydrogen bonds and with the positive charge of the nicotinamide ring of the coenzyme. The C-terminus is acting like an internal inhibitor and makes the active site inaccessible for the substrate. The reduction of the C-terminal disulfide would release the bound terminus and give access for the substrate to the active site. Represented are also the active site Asp201 and the substrate coordinating Arg204.

It has been observed that the activation of the enzyme is slowed down by the presence of oxidized $NADP^+$, a property that remained unexplained until the structure was solved. It is now evident that the negative charges at the C-terminus are responsible for this phenomenon by interacting with the positive charge at the nicotinamide ring of $NADP^+$. The structure of NADP–MDH both with and without cofactor has been solved. In the apo-enzyme a number of interactions stabilize the position of the C-terminal extension between the disulfide and the active site. In the presence of oxidized cofactor the extension gets more tightly anchored through the interaction of the opposite charges, thereby slowing down the reductive activation of the enzyme.

A 15-amino acid-long C-terminal peptide, Ala375–Val389, acquired an increased mobility upon reduction in a monomeric MDH as shown by two-dimensional proton NMR (Krimm *et al*. 1999). The monomeric enzyme was obtained by truncation of 33-amino acids at the N terminus. The direct sequence-specific NMR assignment suggests that the first part of the C-

terminal peptide is still folded near the core of the enzyme, so that cysteines 365 and 377 remain in proximity to allow for an efficient reoxidation/inactivation of the enzyme.

The three-dimensional structure of oxidized NADP-dependent MDHs is a first step towards understanding the conformational rearrangements during the activation of the enzyme. In view of the flexibility of the N-terminal extension, both extensions can be assumed to be flexible in the reduced active structure. The structures of the various partially deregulated mutants lacking some of the disulfides would provide a view of the transient structural modifications the enzyme undergoes during the activation process.

5.1.3 Thioredoxin interactions

Both trx-*f* and trx-*m* as well as *E. coli* thioredoxin can reduce the disulfides of MDH *in vitro*, which means that there is no high specificity for the MDH activation. Under certain conditions trx-*f* is even more efficient in reducing MDH than trx-*m*. It has therefore been proposed that trx-*f* is the prime activator protein of all light-activated enzymes involved in carbon assimilation and regulated by the ferredoxin/thioredoxin system (Schürmann & Buchanan, 2000; Schürmann & Jacquot, 2000). Docking studies with different thioredoxin structures demonstrate that both disulfides of MDH are accessible enough for reduction to occur.

5.2 Fructose-1,6-bisphosphatase

One of the four light regulated key enzymes of the Calvin cycle is chloroplastic FBPase, which catalyzes the conversion of fructose-1,6-bisphosphate (F-1,6-P) to fructose-6-phosphate (F-6-P). The structure of spinach chloroplast FBPase was solved in 1995 (Villeret *et al*. 1995a), but no regulatory disulfide was visible in the structure which therefore provided little information on how the oxidized enzyme is inactivated. In the light of the recently solved pea chloroplast enzyme structure (Chiadmi *et al*. 1999) and of its conformational similarity to gluconeogenic FBPases, it is plausible to propose that the spinach enzyme structure might correspond to the reduced, active form of the enzyme.

Now the structure of the oxidized form of pea FBPase has been determined to a resolution of 2·2 Å (Chiadmi *et al*. 1999). It shows the regulatory disulfide bridge and provides evidence how the enzyme is reductively regulated (Fig. 20). The FBPase is a homotetramer, composed of a dimer of dimers. The overall structure is similar to that of the cytosolic, gluconeogenic enzyme from pig, whose structure in its active and inactive forms have been thoroughly investigated (Ke *et al*. 1990; Liang *et al*. 1992; Villeret *et al*. 1995b; Choe *et al*. 1998; Weeks *et al*. 1999). The mode of regulation is however distinctly different between the two enzymes. In gluconeogenic FBPase, the activity is allosterically regulated by AMP with only small changes in the active site. In the chloroplastic enzyme the regulation is achieved by switching from an inactive conformation of the active site, stabilized through the regulatory disulfide bridge, to a catalytically competent conformation through reduction of the disulfide bridge. The activation of FBPase is in addition dependent on other light-induced changes in the chloroplasts such as pH and Mg^{2+} levels.

In contrast to the gluconeogenic FBPases, the chloroplastic FBPases contain an amino acid insertion varying from 14 to 19 residues between species. This insertion contains three

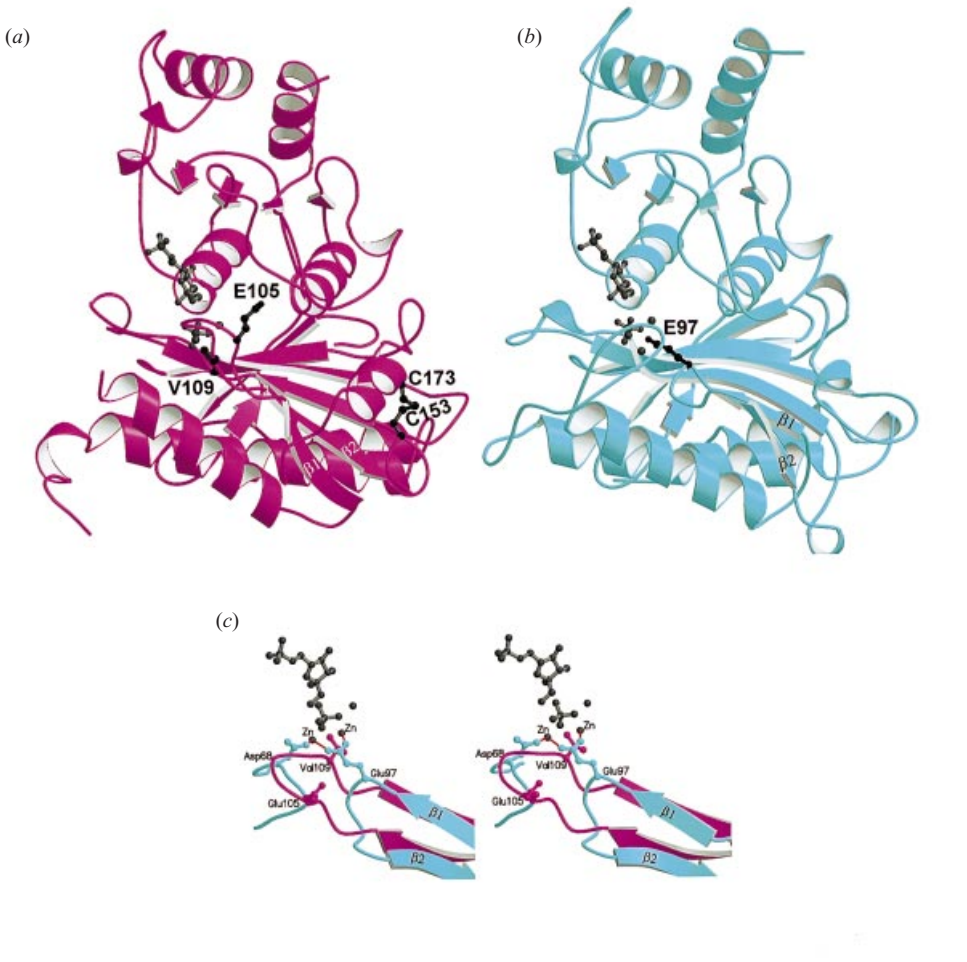

Fig. 20. Comparison of chloroplastic and gluconeogenic FBPase. (*a*) Oxidized pea chloroplastic FBPase (pdb code 1dcu). The disulfide between Cys153 and Cys173 as well as the positions of the catalytic Glu105 and Val109 are shown. The shown fructose-6-phosphate, Pi and Zn^{2+} are modeled according to the positions in the pig enzyme. (*b*) Pig gluconeogenic FBPase in complex with fructose-6-phosphate, Pi and Zn^{2+} (pdb code 1cnq). The catalytic Glu97 is shown. (*c*) The catalytic Glu97 of the pig enzyme (in cyan) is together with Asp68 coordinating two zinc ions. In oxidized pea FBPase (in magenta) the movement of strands β1/β2 removes Glu105, corresponding to the zinc coordinating Glu97 in the pig FBPase, from the active site and positions Val109 near the location of the cation binding site.

conserved cysteines, two of which are involved in the regulatory disulfide. Mutations of these three cysteines result in a partial or total loss of activation (Jacquot *et al*. 1997; Rodriguez-Suarez *et al*. 1997; Y. Balmer *et al*. unpublished). From the structure, it is clear that the regulatory disulfide is formed between Cys153 and Cys173 (pea numbering) and that the third, Cys178, is located on the buried side of the following helix.

If the active site of the gluconeogenic and the chloroplastic FBPases are superimposed, most of the important catalytic residues are occupying similar positions, except for Glu105 (Glu97 in pig enzyme) which is a critical ligand for the catalytic divalent Mg ions. Here a dramatic conformational change is observed where the residues 95–118, which form strands

β1 and β2 of the N-terminal β-sheet, have moved a distance of some 8 Å towards the active site. This movement displaces Glu105 from the active site and its position is instead occupied by Val109, thereby preventing the coordination of the divalent ions. In addition, the position of the loop binding the product F6P-Pi-complex is now partly occupied by the two β-strands. In summary, the movement of the β-strands into the active site results in a dysfunctional binding site for catalytic divalent ions. These conclusions are consistent with the observed Mg^{2+} dependencies of oxidized and reduced FBPase (Schürmann & Wolosiuk, 1978) as well as of some mutants (Y. Balmer *et al*. unpublished).

The function of the insertion in activation can be deduced quite well. When the disulfide is oxidized, the insertion is stable, packing directly against the β1, β2-strands. This stabilizes the position of the β-strands in the active site. Upon reduction of the disulfide by thioredoxin, the insertion is destabilized, as seen in the spinach structure, and the strands are released. This would allow the strands to move back upon substrate binding, enabling the active site residues to adopt their conformations favorable for catalysis, thus yielding a fully active enzyme.

5.3 Redox regulation of chloroplast target enzymes

The redox regulation of FBPase is distinctly different from the regulation of NADP–MDH in that the regulatory insertion does not interact directly with the active site, but rather it stabilizes the inactive conformation. This could explain why, under certain *in vitro* conditions, there is still a low residual activity in the oxidized FBPase, compared to oxidized NADP–MDH, which is totally inactive. Interestingly, in both enzymes the redox active disulfides are at the surface of the enzyme, remote from the active site, making them accessible to reduced thioredoxin. The signal for activation is then conveyed in different ways in the different enzymes to the active sites, which can then adopt their catalytic conformations.

6. Conclusion

Light does not only provide reducing power and ATP for the photosynthetic carbon assimilation, but it also regulates the activity of key photosynthetic enzymes through reduction–oxidation of protein disulfides. This redox regulation is achieved by the ferredoxin : thioredoxin system which is composed of ferredoxin, ferredoxin : thioredoxin reductase (FTR) and thioredoxins which transmits the redox signal from the photosystem to target enzymes. FTR is the key electron/thiol transducer enzyme in this pathway and is unique in that it can reduce its disulfide bridge directly using an iron–sulfur cluster. The structure of the enzyme was recently determined and provides the framework for this reduction revealing close contacts between the iron–sulfur center and the disulfide. The structure of FTR and its functional implication is the central subject of this review and interacting ferredoxin and thioredoxins are discussed in view of this structure. The unusually thin concave disk-like molecule is easily accessible from the 'front' side to a ferredoxin, which can transfer an electron to the disulfide via the iron–sulfur center. Because complete reduction of thioredoxin needs two electrons, a one-electron reduced intermediate, with a unique five-

coordinated iron–sulfur center and a FTR-thioredoxin mixed disulfide are suggested to be formed where thioredoxin is bound to the 'back' side of the FTR. Such an intermediate has a significantly lower redox potential similar to five-coordinated model compounds. The second electron, needed for the complete reduction of thioredoxins, can be delivered by a new ferredoxin from the 'front' side of the FTR molecule. The three-dimensional structures of the chloroplast thioredoxins and the oxidized target enzymes NADP-dependent malate dehydrogenase and fructose-1,6-bisphosphatase have recently also been determined which starts getting the structural basis for redox activation of these enzymes.

7. Acknowledgments

This work was supported by grants from the Swedish Council for Forestry and Agricultural Research and Swedish Natural Science Research Council (to H. E.) and the Schweizerischer Nationalfonds (31-47107.96 to P. S.).

8. References

Adman, E., Watenpaugh, K. D. & Jensen, L. H. (1975). NH–S hydrogen bonds in *Peptococcus aerogenes* ferredoxin, *Clostridium pasteurianum* rubredoxin, and Chromatium high potential iron protein. *Proc. natn. Acad. Sci. USA* **72**, 4854–4858.

Åslund, F. & Beckwith, J. (1999a). Bridge over troubled waters: sensing stress by disulfide bond formation. *Cell* **96**, 751–753.

Åslund, F. & Beckwith, J. (1999b). The thioredoxin superfamily: redundancy, specificity, and gray-area genomics. *J. Bacteriol.* **181**, 1375–1379.

Backes, G., Mino, Y., Loehr, T. M., Mayer, T. E., Casanovich, M. A., Sweeney, W. V., Adman, E. T. & Sanders-Loehr, J. (1991). The environment of Fe_4S_4 clusters in ferredoxin and high-potential iron proteins. New information from X-ray crystallography and resonance Raman spectroscopy. *J. Am. chem. Soc.* **113**, 2055–2064.

Ballicora, M. A., Frueauf, J. B., Fu, Y., Schürmann, P. & Preiss, J. (2000). Activation of the potato tuber ADP-glucose pyrophosphorylase by thioredoxin. *J. biol. Chem.* **275**, 1315–1320.

Barber, J. & Andersson, B. (1994). Revealing the blueprint of photosynthesis. *Nature* **370**, 31–34.

Baumann, B., Sticht, H., Scharpf, M., Sutter, M., Haehnel, W. & Rosch, P. (1996). Structure of *Synechococcus elongatus* [Fe2S2] ferredoxin in solution. *Biochemistry* **35**, 12831–12841.

Beinert, H., Holm, R. H. & Munck, E. (1997). Iron–sulfur clusters: nature's modular, multipurpose structures. *Science* **277**, 653–659.

Bes, M. T., Parisini, E., Inda, L. A., Saraiva, L. M., Peleato, M. L. & Sheldrick, G. M. (1999). Crystal structure determination at 1·4 Å resolution of ferredoxin from the green alga *Chlorella fusca*. *Structure Fold. Des.* **7**, 1201–1211.

Binda, C., Coda, A., Aliverti, A., Zanetti, G. & Mattevi, A. (1998). Structure of the mutant E92K of [2Fe–2S] ferredoxin I from *Spinacia oleracea* at 1·7 Å resolution. *Acta crystallogr.* **D54**, 1353–1358.

Birktoft, J. J., Rhodes, G. & Banaszak, L. J. (1989). Refined crystal structure of cytoplasmic malate dehydrogenase at 2·5-Angstroms resolution. *Biochemistry* **28**, 6065–6081.

Brandes, H. K., Hartman, F. C., Lu, T. Y. & Larimer, F. W. (1996). Efficient expression of the gene for spinach phosphoribulokinase in *Pichia pastoris* and utilization of the recombinant enzyme to explore the role of regulatory cysteinyl residues by site-directed mutagenesis. *J. biol. Chem.* **271**, 6490–6496.

Bruschi, M. & Guerlesquin, F. (1988). Structure, function and evolution of bacterial ferredoxins. *FEMS microbiol. Rev.* **4**, 155–175.

Buchanan, B. B. (1980). Role in the light in the regulation of chloroplast enzymes. *A. Rev. Pl. Physiol.* **31**, 341–364.

Buchanan, B. B. (1991). Regulation of CO_2 assimilation in oxygenic photosynthesis: the ferredoxin/thioredoxin system. Perspective on its discovery, present status, and future development. *Archs Biochem. Biophys.* **288**, 1–9.

Buchanan, B. B., Schürmann, P., Decottignies, P. & Lozano, R. M. (1994). Thioredoxin: A multifunctional regulatory protein with a bright future in technology and medicine. *Archs Biochem. Biophys.* **314**, 257–260.

Capitani, G., Markovic-Housley, Z., del Val, G., Morris, M., Jansonius, J. N. & Schürmann, P. (2000). Crystal structures of two functionally different thioredoxins in spinach chloroplasts. *J. molec. Biol.* (in press).

Carr, P. D., Verger, D., Ashton, A. R. & Ollis, D. L. (1999). Chloroplast NADP-malate dehydrogenase: structural basis of light-dependent regulation of activity by thiol oxidation and reduction. *Structure* **7**, 461–475.

Chapman, A. D., Cortes, A., Dafforn, T. R., Clarke, A. R. & Brady, R. L. (1999). Structural basis of substrate specificity in malate dehydrogenases: Crystal structure of a ternary complex of porcine cytoplasmic malate dehydrogenase, alpha-ketomalonate and tetrahydonad. *J. molec. Biol.* **285**, 703–712.

Chiadmi, M., Navaza, A., Miginiac-Maslow, M., Jacquot, J.-P. & Cherfils, J. (1999). Redox signalling in the chloroplast: structure of oxidized pea fructose-1,6-bisphosphate phosphatase. *EMBO J.* **18**, 6809–6815.

Choe, J. Y., Poland, B. W., Fromm, H. J. & Honzatko, R. B. (1998). Role of a dynamic loop in cation activation and allosteric regulation of recombinant porcine fructose-1,6-bisphosphatase. *Biochemistry* **37**, 11 441–11 450.

Ciurli, S., Carrie, M., Weigel, J. A., Carney, M. J., Stack, T. D. P., Papaefthymiou, G. C. & Holm, R. H. (1990). Subsite-differentiated analogues of native $[4Fe–4S]^{2+}$ clusters: Preparation of clusters with five- and six-coordinate subsites and modulation of redox potentials and charge distributions. *J. Am. chem. Soc.* **112**, 2654–2664.

Dai, S., Saarinen, M., Ramaswamy, S., Meyer, Y., Jacquot, J. P. & Eklund, H. (1996). Crystal structure of *Arabidopsis thaliana* NADPH dependent thioredoxin reductase at 2·5 Å resolution. *J. molec. Biol.* **264**, 1044–1057.

Dai, S. D., Schwendtmayer, C., Ramaswamy, S., Eklund, H. & Schürmann, P. (1998). Crystallization and crystallographic investigations of ferredoxin: thioredoxin reductase from *Synechocystis* sp. PCC6803. In: *Photosynthesis: Mechanisms and Effects,* (ed. Garab, G.). Vol. 3, pp. 1931–1934. Kluwer Academic Publishers.

Dai, S., Schwendtmayer, C., Schürmann, P., Ramaswamy, S. & Eklund, H. (2000). Redox signaling in chloroplasts: cleavage of disulfides by an iron–sulfur cluster. *Science* **28**, 655–658.

De La Torre, A., Lara, C., Yee, B. C., Malkin, R. & Buchanan, B. B. (1982). Physiochemical properties of ferralterin, a regulatory iron–sulfur protein functional in oxygenic photosynthesis. *Archs Biochem. Biophys.* **213**, 545–550.

del Val, G., Maurer, F., Stutz, E. & Schürmann, P. (1999). Modification of the reactivity of spinach chloroplast thioredoxin *f* by site-directed mutagenesis. *Plant Sci.* **149**, 183–190.

Droux, M., Miginiac-Maslow, M., Jacquot, J.-P., Gadal, P., Crawford, N. A., Kosower, N. S. & Buchanan, B. B. (1987). Ferredoxin–thioredoxin reductase: a catalytically active dithiol group links photoreduced ferredoxin to thioredoxin functional in photosynthetic enzyme regulation. *Archs Biochem. Biophys.* **256**, 372–380.

Dunford, R. P., Catley, M. A., Raines, C. A., Lloyd, J. C. & Dyer, T. A. (1998). Purification of active chloroplast sedoheptulose-1,7-bisphosphatase expressed in *Escherichia coli*. *Protein Expr. Purif.* **14**, 139–145.

Eklund, H., Gleason, F. & Holmgren, A. (1991). Structural and functional relations among thioredoxins of different species. *Proteins* **11**, 13–28.

Falzone, C. J., Kao, H., Zhao, J., Bryant, D. A. & Lecomte, J. T. (1994). Three-dimensional solution structure of PsaE from the cyanobacterium Synechococcus sp. strain PCC 7002, a photosystem I protein that shows structural homology with SH3 domains. *Biochemistry* **33**, 6052–6062.

Frolow, F., Harel, M., Sussman, J. L., Mevarech, M. & Shoham, M. (1996). Insights into protein adaptation to a saturated salt environment from the crystal structure of a halophilic 2Fe–2S ferredoxin. *Nature struct. Biol.* **3**, 452–458.

Fukuyama, K., Hase, T., Matsumoto, S., Tshukihara, T., Katsube, Y., Tanaka, N., Kakudo, M., Wada, K. & Matsubara, H. (1980). Structure of *S. platensis* [2Fe–2S] ferredoxin and evolution of chloroplast ferredoxins. *Nature* **286**, 522–524.

Fukuyama, K., Ueki, N., Nakamura, H., Tsukihara, T. & Matsubara, H. (1995). Tertiary structure of [2Fe–2S] ferredoxin from *Spirulina platensis* refined at 2·5 Å resolution: structural comparisons of plant-type ferredoxins and an electrostatic potential analysis. *J. Biochem.* (*Tokyo*) **117**, 1017–1023.

Gleason, W. B., Fu, Z., Birktoft, J. J. & Banaszak, L. J. (1994). Refined structure of mitochondrial malate dehydrogenase from porcine heart and the consensus structure for dicarboxylic acid oxidoreductases. *Biochemistry* **33**, 2078–2088.

Harrison, P. M. & Sternberg, M. J. E. (1996). The disulfide β-cross: from cystine geometry and clustering to classification of small disulfide rich protein folds. *J. molec. Biol.* **264**, 603–623.

Hatch, M. D. (1987). C4 photosynthesis: A unique blend of modified biochemistry, anatomy and Ultrastructure. *Biochem. biophys. Acta.* **895**, 81–106.

Hirasawa, M., Droux, M., Gray, K. A., Boyer, J. M., Davis, D. J., Buchanan, B. B. & Knaff, D. B. (1988). Ferredoxin-thioredoxin reductase: properties of its complex with ferredoxin. *Biochim. biophys. Acta.* **935**, 1–8.

Hirasawa, M., Schürmann, P., Jacquot, J.-P., Manieri, W., Jacquot, P., Keryer, E., Hartman, F. C. & Knaff, D. B. (1999). Oxidation–reduction properties of chloroplast thioredoxins, ferredoxin: thioredoxin reductase and thioredoxin f-regulated enzymes. *Biochemistry* **38**, 5200–5205.

Holmgren, A. (1995). Thioredoxin structure and mechanism: conformational changes on oxidation of the active-site sulfhydryls to a disulfide. *Structure* **3**, 239–243.

Howard, J. B. & Rees, D. C. (1991). Perspective on non-heme iron protein chemistry. *Adv. Protein Chem.* **42**, 199–280.

Hunt, J. F., van der Vies, S. M., Henry, L. & Deisenhofer, J. (1997). Structural adaptations in the specialized bacteriophage T4 co-chaperonin Gp31 expand the size of the Anfinsen cage. *Cell* **90**, 361–371.

Ikemizu, S., Bando, M., Sato, T., Morimoto, Y., Tsukihara, T. & Fukuyama, K. (1994). Crystal structure of [2Fe–2S] ferredoxin I from *Equisetum arvense* at 1·8 Å resolution. *Acta crystallogr.* **D50**, 167–174.

Im, S. C., Liu, G., Luchinat, C., Sykes, A. G. & Bertini, I. (1998). The solution structure of parsley [2Fe–2S] ferredoxin. *Eur. J. Biochem.* **258**, 465–477.

Jacobson, B. L., Chae, Y. K., Markley, J. L., Rayment, I. & Holden, H. M. (1993). Molecular structure of the oxidized, recombinant heterocyst (2Fe–2S) ferredoxin from *Anabaena* 7120 determined to 1·7 Å resolution. *Biochemistry* **32**, 6788–6793.

Jacquot, J.-P., Lancelin, J.-M. & Meyer, Y. (1997). Thioredoxins: structure and function in plant cells. *New Phytol.* **136**, 543–570.

Johansson, K., Ramaswamy, S., Saarinen, M., Lemaire-Chamley, M., Issakidis-Bourguet, E., Miginiac-Maslow, M. & Eklund, H. (1999). Structural basis for light activation of a chloroplast enzyme. The structure of *Sorghum* NADP–malate dehydrogenase in its oxidized form. *Biochemistry* **38**, 4319–4326.

Jones, T. A., Zou, J. Y., Cowan, S. W. & Kjeldgaard, A. (1991). Improved methods for binding protein models in electron density maps and the location of errors in these models. *Acta crystallogr.* **A47**, 110–119.

Ke, H. M., Zhang, Y. P. & Lipscomb, W. N. (1990). Crystal structure of fructose-1,6-bisphosphatase complexed with fructose 6-phosphate, AMP, and magnesium. *Proc. natn. Acad. Sci. USA* **87**, 5243–5247.

Klenk, H. P. *et al.* (1997). The complete genome sequence of the hyperthermophilic sulphate-reducing archaeon *Archaeoglobus fulgidus*. *Nature* **390**, 364–370.

Klukas, O., Schubert, W.-D., Jordan, P., Krauss, N., Fromme, P., Witt, H. T. & Saenger, W. (1999a). Photosystem I, an Improved Model of the Stromal Subunits PsaC, PsaD, and PsaE. *J. biol. Chem.* **274**, 7351–7360.

Klukas, O., Schubert, W.-D., Jordan, P., Krauss, N., Fromme, P., Witt, H. T. & Saenger, W. (1999b). Localization of two phylloquinones, QK and QK′, in an improved electron density map of photosystem I at 4-Å resolution. *J. biol. Chem.* **274**, 7361–7367.

Knaff, D. B. (1996). Ferredoxin and ferredoxin-dependent enzymes. In *Advances in Photosynthesis* (eds Yocum, C. F. & Ort, D. R.), pp. 333–361. Kluwer Academic Publishers, Dordrecht.

Krauss, N., Schubert, W. D., Klukas, O., Fromme, P., Witt, H. T. & Saenger, W. (1996). Photosystem I at 4 Å resolution represents the first structural model of a joint photosynthetic reaction center and core antenna system. *Nat. struct. Biol.* **3**, 965–973.

Krimm, I., Goyer, A., Issakidis-Bourguet, E., Miginiac-Maslow, M. & Lancelin, J. M. (1999). Direct NMR observation of the thioredoxin-mediated reduction of the chloroplast NADP–malate dehydrogenase provides a structural basis for the relief of autoinhibition. *J. biol. Chem.* **274**, 34539–34542.

Kuo, C. F., McRee, D. E., Fisher, C. L., O'Handley, S. F., Cunningham, R. P. & Tainer, J. A. (1992). Atomic structure of the DNA repair [4Fe–4S] enzyme endonuclease III. *Science* **16**, 258, 434–440.

Lancelin, J. M., Stein, M. & Jacquot, J. P. (1993). Secondary structure and protein folding of recombinant chloroplastic thioredoxin Ch2 from the green alga *Chlamydomonas reinhardtii* as determined by ^{1}H NMR. *J. Biochem.* (*Tokyo*) **114**, 421–431.

Lancelin, J. M., Guilhaudis, L., Krimm, I., Blackledge, M. J., Marion, D. & Jacquot, J. P. NMR structure and dynamic of the chloroplast thioredoxin M Ch2 from the green alga Chlamydomonas Reinhardtii (to be published).

Langen, R., Jensen, G. M., Jacob, U., Stephens, P. J. & Warshel, A. (1992). Protein control of iron-sulfur cluster redox potentials. *J. biol. Chem.* **267**, 25625–25627.

Lelong, C., Setif, P., Bottin, H., Andre, F. & Neumann, J. M. (1995). ^{1}H and ^{15}N NMR sequential assignment, secondary structure, and tertiary fold of [2Fe–2S] ferredoxin from *Synechocystis* sp. PCC 6803. *Biochemistry* **34**, 14462–14473.

Lelong, C., Boekema, E. J., Kruip, J., Bottin, H., Rogner, M. & Setif, P. (1996). Characterization of a redox active cross-linked complex between cyanobacterial photosystem I and soluble ferredoxin. *EMBO J.* **15**, 2160–2168.

Lendzian, K. & Ziegler, H. (1970). Über die Regulation der Glucose-6-phosphat-Dehydrogenase in Spinatchloroplasten durch Licht. *Planta* **94**, 27–36.

Liang, J. Y., Huang, S., Zhang, Y., Ke, H. & Lipscomb, W. N. (1992). Crystal structure of the neutral form of fructose 1,6-bisphosphatase complexed with regulatory inhibitor fructose 2,6-bisphosphate at 2·6-Å resolution. *Proc. natn. Acad. Sci. USA* **89**, 2402–2408.

Mayer, K. L., Shen, G., Bryant, D. A., Lecomte, J. T. & Falzone, C. J. (1999). The solution structure of photosystem I accessory protein E from the cyanobacterium *Nostoc* sp. strain PCC 8009. *Biochemistry* **38**, 13736–13746.

Meyer, Y., Verdoucq, L. & Vignols, F. (1999). Plant thioredoxins and glutaredoxins: identity and putative roles. *Trends Plant Sci*. **4**, 388–394.

Miginiac-Maslow, M., Issakidis, E., Lemaire, M., Ruelland, E., Jacquot, J. P. & Decottignies, P. (1997). Light-dependent activation of NADP–malate dehydrogenase: a complex process. *Aust. J. Pl. Physiol*. **24**, 529–542.

Mills, J. D., Mitchell, P. & Schürmann, P. (1980). Modulation of coupling factor ATPase activity in intact chloroplasts. The role of the thioredoxin system. *FEBS Lett*. **112**, 173–177.

Morales, R., Chron, M.-H., Hudry-Clergeon, G., Petillot, Y., Norager, S., Medina, M. & Frey, M. (1999). Refined X-ray structures of the oxidized, at 1·3 Å, and reduced, at 1·17 Å, [2Fe–2S] ferredoxin from the cyanobacterium *Anabaena* PCC7119 show redox-linked conformational changes. *Biochemistry* **38**, 15764.

Muhlenhoff, U., Kruip, J., Bryant, D. A., Rogner, M., Setif, P. & Boekema, E. (1996). Characterization of a redox-active cross-linked complex between cyanobacterial photosystem I and its physiological acceptor flavodoxin. *EMBO J*. **15**, 488–497.

Porter, M. A., Stringer, C. D. & Hartman, F. C. (1988). Characterization of the regulatory thioredoxin site of phosphoribulokinase. *J. biol. Chem*. **263**, 123–129.

Powis, G., Kirkpatrick, D. L., Angulo, M. & Baker, A. (1998). Thioredoxin redox control of cell growth and death and the effects of inhibitors. *Chem. Biol. Interact*. **111–112**, 23–24.

Richardson, J. S. (1981). The anatomy and taxonomy of protein structure. *Adv. protein Chem*. **34**, 167–339.

Rodriguez-Suarez, R. J., Mora-Garcia, S. & Wolosiuk, R. A. (1997). Characterization of cysteine residues involved in the reductive activation and the structural stability of rapeseed (*Brassica napus*) chloroplast fructose-1,6-bisphosphatase. *Biochem. Biophys. Res. Common*. **232**, 388–393.

Rypniewski, W. R., Breiter, D. R., Benning, M. M., Wesenberg, G., Oh, B.-H., Markley, J. L., Rayment, I. & Holden, H. M. (1991). Crystallization and structure determination to 2·5-Å resolution of the oxidized [2Fe–2S] ferredoxin isolated from *Anabaena* 7120. *Biochemistry* **30**, 4126–4131.

Saarinen, M., Gleason, F. K. & Eklund, H. (1995). Crystal structure of thioredoxin-2 from *Anabaena*. *Structure* **3**, 1097–1108.

Salamon, Z., Tollin, G., Hirasawa, M., Knaff, D. B. & Schürmann, P. (1995). The oxidation–reduction properties of spinach thioredoxins f and m and of ferredoxin:thioredoxin reductase. *Biochim. biophys. Acta Bio-Energetics* **1230**, 114–118.

Schubert, W. D., Klukas, O., Saenger, W., Witt, H. T., Fromme, P. & Krauss, N. (1998). A common ancestor for oxygenic and anoxygenic photosynthetic systems: a comparison based on the structural model of photosystem I. *J. molec. Biol*. **280**, 297–314.

Schürmann, P. (1981). The ferredoxin/thioredoxin system of spinach chloroplasts. Purification and characterization of its components. In *Photosynthesis IV. Regulation of carbon metabolism* (ed. Akoyunoglou, G.) pp. 273–280. Philadelphia, Pa: Balaban Intern. Sci. Services.

Schürmann, P. & Wolosiuk, R. A. (1978). Studies on the regulatory properties of chloroplast fructose-1,6-bisphosphatase. *Biochim. biophys. Acta* **522**, 130–138.

Schürmann, P. & Gardet-Salvi, L. (1993). Chemical modification of the active site of ferredoxin–thioredoxin reductase. *Chimia* **47**, 245–246.

Schürmann, P. & Buchanan, B. B. (2000). The structure and function of the ferredoxin/thioredoxin system. In: *Regulatory Aspects of Photosynthesis. Advances in Photosynthesis*, (eds Andersson, B. & Aro, E. M.). Kluwer Academic Publishers, Dordrecht, The Netherlands (in press).

Schürmann, P. & Jacquot, J.-P. (2000). Plant thioredoxin systems revisited. *A. Rev. Plant Physiol. Plant molec. Biol*. **51** (in press).

Schwarz, O., Schürmann, P. & Strotmann, H. (1997). Kinetics and thioredoxin specificity of thiol modulation of the chloroplast H^+-ATPase. *J. biol. Chem*. **272**, 16924–16927.

Schwendtmayer, C., Manieri, W., Hirasawa, M., Knaff, D. B. & Schürmann, P. (1998). Cloning, expression and characterization of ferredoxin:thioredoxin reductase from *Synechocystis* sp. PCC6803. In *Photosynthesis: Mechanisms and Effects* (*Proceedings of the XIth International Congress on Photosynthesis*, *Budapest*, *Hungary*) (ed. Garab, G.). Kluwer Academic Publishers, Dordrecht, The Netherlands.

Sétif, P., Hanely, J., Barth, P., Bottin, H. & Lagoutte, B. (1995). In *Photosynthesis: From Light to Biosphere. Proceedings of the 10th International Conference on Photosynthesis*, *Montpellier*, *1995* (ed. Mathis, P.) Vol. II, pp. 23–28. Kluwer Academic, Dordrecht, The Netherlands.

Smith, D. R. *et al*. (1997). Complete genome sequence of Mathanobacterium thermoautotropicum delta H: functional analysis and comparative genomics. *J. Bacteriol*. **179**, 7135–7155.

Staples, C. R., Ameyibor, E., Fu, W., Gardet-Salvi, L., Stritt-Etter, A.-L., Schürmann, P., Knaff, D. B. & Johnson, M. K. (1996). The nature and properties of the iron–sulfur center in spinach ferredoxin:thioredoxin reductase: a new biological role for iron–sulfur clusters. *Biochemistry* **35**, 11425–11434.

Staples, C. R., Gaymard, E., Stritt-Etter, A. L., Telser, J., Hoffmann, B. M., Schürmann, P., Knaff, D. B. & Johnson, M. K. (1998). Role of the $[Fe_4S_4]$ cluster in mediating disulfide reduction in

spinach ferredoxin : thioredoxin reductase. *Biochemistry* **37**, 4612–4620.

Stout, C. D., Stura, E. A. & McRee, D. E. (1998). Structure of *Azobacter vinelandii* 7Fe ferredoxin at 1·35 Å resolution and the determination of the [Fe–S] bonds with 0·01 Å accuracy. *J. molec. Biol.* **278**, 629–639.

Thompson, J. D., Plewniak, F., Jeanmougin, F. & Higgins, D. G. (1997). The ClustalX windows interface: flexible strategies for multiple sequence alignment aided by quality analysis tools. *Nucleic Acids Res.* **25**, 4876–4882.

Tsugita, A., Maeda, K. & Schürmann, P. (1983). Spinach chloroplast thioredoxins in evolutionary drift. *Biochem. Biophys. Res. Commun.* **115**, 1–7.

Tsukihara, T., Fukuyama, K., Mizushima, M., Harioka, T., Kusunoki, M., Katsube, Y., Hase, T. & Matsubara, H. (1990). Structure of the [2Fe–2S] ferredoxin I from the blue-green alga *Aphanothece sacrum* at 2·2 Å resolution. *J. molec. Biol.* **216**, 399–410.

van Thor, J. J., Geerlings, T. H., Matthijs, H. C. P. & Hellingwerf, K. J. (1999). Kinetic evidence for the PsaE-dependent transient ternary complex photosystem I/ferredoxin/ferredoxin : $NADP^+$ reductase in a cyanobacterium. *Biochemistry* **38**, 12735–12746.

Villeret, V., Huang, S., Zhang, Y., Xue, Y. & Lipscomb, W. N. (1995a). Crystal structure of spinach chloroplast fructose-1,6-bisphosphatase at 2·8 Å resolution. *Biochemistry* **34**, 4299–4306.

Villeret, V., Huang, S., Zhang, Y. & Lipscomb, W. N. (1995b). Structural aspects of the allosteric inhibition of fructose-1,6-bisphosphatase by AMP: the binding of both the substrate analogue 2,5-anhydro-D-glucitol 1,6-bisphosphate and catalytic metal ions monitored by X-ray crystallography. *Biochemistry* **34**, 4307–4315.

Weeks, C. M., Roszak, A. W., Erman, M., Kaiser, R., Jornvall, H. & Ghosh, D. (1999). Structure of rabbit liverfructose 1,6-bisphosphatase at 2·3 Å resolution. *Acta crystallogr.* **D55**, 93–102.

Wenderoth, I., Scheibe, R. & von Schaewen, A. (1997). Identification of the cysteine residues involved in redox modification of plant plastidic glucose-6-phosphate dehydrogenase. *J. biol. Chem.* **272**, 26985–26990.

Williams, C. H. Jr. (1992). In *Chemistry and Biochemistry of Flavoenzymes* (ed. Müller, F.) Vol. III, pp. 121–211. CRC Press, Boca Raton, FL.

Wu, X., Knudsen, B., Feller, S. M., Zheng, J., Sali, A., Cowburn, D., Hanafusa, H. & Kuriyan, J. (1995). Structural basis for the specific interaction of lysine-containing proline-rich peptides with the N-terminal SH3 domain of c-Crk. *Structure* **3**, 215–226.

Xu, Z., Horwich, A. L. & Sigler, P. B. (1997). The crystal structure of the asymmetric GroEL–GroES–(ADP)7 chaperonin complex. *Nature* **388**, 741–750.

Zhang, N. & Portis, A. R. Jr. (1999). Mechanism of light regulation of Rubisco: A unique role for the larger Rubisco activase isoform involving reductive activation by thioredoxin-f. *Proc. natn. Acad. Sci. USA* **96**, 9438–9443.